Quaternary Science Reviews 39 (2012) 45–59

Contents lists available at SciVerse ScienceDirect

Quaternary Science Reviews

journal homepage: www.elsevier.com/locate/quascirev

Quantitative estimation of Holocene surface salinity variation in the Black Sea using dinoflagellate cyst process length

Kenneth Neil Mertens [a,*], Lee R. Bradley [b], Yoshihito Takano [c], Petra J. Mudie [d,e], Fabienne Marret [b], Ali E. Aksu [e], Richard N. Hiscott [e], Thomas J. Verleye [a], Erik A. Mousing [f], Ludmila L. Smyrnova [g], Siamak Bagheri [h,i], Mashhor Mansor [i], Vera Pospelova [j], Kazumi Matsuoka [c]

[a] Research Unit Palaeontology, Ghent University, Krijgslaan 281 S8, 9000 Gent, Belgium
[b] School of Environmental Sciences, University of Liverpool, Liverpool L69 7ZT, UK
[c] Institute for East China Sea Research (ECSER), 1-14, Bunkyo-machi, Nagasaki 852-8521, Japan
[d] Geological Survey Canada Atlantic, Dartmouth, Nova Scotia B2Y 4A2, Canada
[e] Earth Sciences Department, Memorial University of Newfoundland, St. John's, Newfoundland A1B 3X5, Canada
[f] Center for Macroecology, Evolution and Climate, Department of Biology, University of Copenhagen, Universitetsparken 15, DK-2100 Copenhagen Ø, Denmark
[g] Research Centre "State Oceanarium", 7, Epronovskaya str., Sevastopol 99024, Ukraine
[h] Inland Waters Aquaculture Institute, Iranian Fisheries Research Organization (IFRO), 66 Anzali, Iran
[i] School of Biological Sciences, Universiti Sains Malaysia, 11800 Penang, Malaysia
[j] School of Earth and Ocean Sciences, University of Victoria, OEASB A405, P.O. Box 3065 STN CSC, Victoria, BC V8W 3V6, Canada

ARTICLE INFO

Article history:
Received 10 May 2011
Received in revised form
24 January 2012
Accepted 27 January 2012
Available online xxx

Keywords:
Paleosalinity
Lingulodinium machaerophorum
rDNA analysis
Caspian Sea
Sea of Azov
Black Sea
Marmara Sea

ABSTRACT

Reconstruction of salinity in the Holocene Black Sea has been an ongoing debate over the past four decades. Here we calibrate summer surface water salinity in the Black Sea, Sea of Azov and Caspian Sea with the process length of the dinoflagellate cyst *Lingulodinium machaerophorum*. We then apply this calibration to make a regional reconstruction of paleosalinity in the Black Sea, calculated by averaging out process length variation observed at four core sites from the Black Sea with high sedimentation rates and dated by multiple mollusk shell ages. Results show a very gradual change of salinity from ~14 ± 0.91 psu around 9.9 cal ka BP to a minimum ~12.3 ± 0.91 psu around 8.5 cal ka BP, reaching current salinities of ~17.1 ± 0.91 psu around 4.1 cal ka BP. The resolution of our sampling is about 250 years, and it fails to reveal a catastrophic salinization event at ~9.14 cal ka BP advocated by other researchers. The dinoflagellate cyst salinity-proxy does not record large Holocene salinity fluctuations, and after early Holocene freshening, it shows correspondence to the regional sea-level curve of Brückner et al. (2010) derived from Balabanov (2007).

1. Introduction

It has been suggested that during the Holocene, the Black Sea changed rapidly from a freshwater – brackish environment into higher salinity conditions during a catastrophic megaflood event around 7.5 cal ka BP, called 'Noah's flood' (Ryan et al., 1997). The age of this suggested megaflood event was later changed to 9.4 cal ka BP by Ryan et al. (2003). They converted their raw radiocarbon estimate of the timing of the flood (8.4 ^{14}C ka) to calendar years using a reservoir age of zero years. In this paper, we have recalibrated their raw age using a reservoir age of 300 years (Soulet et al., 2011; procedures explained in Table 1 and applied to all radiocarbon dates in this paper); with this revised calibration procedure, the date of the proposed megaflood event is reduced to ~9.14 cal ka BP. According to the hypothesis of Ryan and coworkers, the sudden input of saltwater at ~9.14 cal ka BP resulted in an abrupt increase of salinity and rapid rise of the water level from a depth of more than 100 m below sea level (Ryan and Pitman, 1998). Conflicting evidence was presented by Aksu et al. (2002a,b), Hiscott et al. (2002) and Mudie et al. (2001, 2002, 2004) who hypothesized persistent early Holocene outflow of brackish water from the Black Sea into the Marmara Sea before the

* Corresponding author. Tel.: +32 92644613; fax: +32 92644608.
E-mail addresses: kenneth.mertens@ugent.be (K.N. Mertens), l.r.bradley@liverpool.ac.uk (L.R. Bradley), takadino@gmail.com (Y. Takano), pmudie@nrcan.gc.ca (P.J. Mudie), f.marret@liv.ac.uk (F. Marret), aaksu@mun.ca (A.E. Aksu), rhiscott@mun.ca (R.N. Hiscott), thomas.verleye@ugent.be (T.J. Verleye), eamousing@bio.ku.dk (E.A. Mousing), inik48@inbox.ru (L.L. Smyrnova), siamakbp@gmail.com (S. Bagheri), mashhor@usm.my (M. Mansor), vpospe@uvic.ca (V. Pospelova), kazu-mtk@nagasaki-u.ac.jp (K. Matsuoka).

0277-3791/$ – see front matter © 2012 Elsevier Ltd. All rights reserved.
doi:10.1016/j.quascirev.2012.01.026

Table 1
Radiocarbon ages with increasing depth in the composite stratigraphy at four core sites in the Black Sea, reported as uncalibrated conventional ^{14}C dates in yr BP (half-life of 5568 years; errors are 68.3% confidence limits) and calibrated calendar ages (cal yr BP) determined with Oxcal4.0 online software, Marine09.14c calibration curve. We use a reservoir age of 415 yr (Siani et al., 2000) for all raw dates younger than 7.1 ^{14}C ka. We use a reservoir age of 300 yr for all raw dates older than 8.4 ^{14}C ka in shelf cores MAR02-45, MAR05-04G and MAR05-13P, consistent with Soulet et al. (2011). 7.1 ^{14}C ka and 8.4 ^{14}C ka are, respectively, the times of euryhaline mollusc appearance and first influence of Mediterranean water identified by Ryan et al. (1997) and Ryan et al. (2003). For raw shell dates between 7.1 ^{14}C ka and 8.4 ^{14}C ka in shelf cores, we use linear interpolation to obtain an appropriate reservoir age between 300 yr and 415 yr. For our two deep-water sites, we use a reservoir age of 1000 yr prior to 7.5 ^{14}C ka and 415 yr for younger raw dates. Prior to 7.1–7.5 ^{14}C ka, the reservoir values are different for shelf sites and deep-water sites because of water-column stratification (Kwiecien et al., 2008). Laboratory numbers bear the prefix "TO" for IsoTrace Radiocarbon Laboratory, Accelerator Mass Spectrometry Facility, University of Toronto, the prefix "UCIAMS" for Radiocarbon Dating Laboratory, Université Laval, and the prefix "KIA" for Leibniz-Labor für Altersbestimmung und Isotopenforschung of the University of Kiel. Extrapolated ages on either side of unconformities α_1 and α_2 have error bars consistent with all combinations of ±errors of the two radiocarbon ages above and below that level.

Core	Depth (cm)	Composite depth (cm)	Water depth (m)	Dated material	^{14}C date (year BP)	Calendar age (cal yr BP)	Lab No./Reference
MAR 02-45T	0	0	69	Modern core top	415 ± 90	0	Reservoir age
MAR 02-45T	92	92	69	*Spisula subtruncata*	730 ± 50	365 ± 50	TO-11433
MAR 02-45P	33	143	69	*Spisula subtruncata*	730 ± 40	365 ± 45	TO-11435
MAR 02-45T	145	145	69	*Spisula subtruncata*	770 ± 50	395 ± 55	TO-11434
MAR 02-45P	158	268	69	*Mytilus edulis*	2400 ± 60	2025 ± 80	TO-11006
MAR 02-45P	160	270	69	Just above α_2	2425 ± 60	2050 ± 80	Extrapolation
MAR 02-45P	161	271	69	Just below α_2	5095 ± 25	5465 ± 55	Extrapolation
MAR 02-45P	174	284	69	*Mytilus galloprovincialis*	5115 ± 20	5480 ± 45	UCIAMS-85907
MAR 02-45P	220	330	69	*Mytilus edulis*	5190 ± 50	5535 ± 55	TO-11436
MAR 02-45P	302	412	69	*Mytilus galloprovincialis*	5900 ± 60	6310 ± 65	TO-11437
MAR 02-45P	406	516	69	*Monodacna pontica*	7560 ± 60	8055 ± 65	TO-11438
MAR 02-45P	495	605	69	*Truncatella subcylindrica*	8380 ± 70	9120 ± 95	TO-11142
MAR 02-45P	569	679	69	*Didacna ?praetrigonoides*	8570 ± 70	9335 ± 85	TO-11439
MAR 02-45P	639	749	69	*Didacna* spp.	8620 ± 70	9385 ± 75	TO-11440
MAR 02-45P	754	864	69	*Dreissena rostiformis*	8840 ± 70	9635 ± 100	TO-11441
MAR 02-45P	810	920	69	*Dreissena rostiformis*	9370 ± 70	10,335 ± 80	TO-11007
MAR 05-04G	0	0	75	Modern core top	415 ± 90	0	Reservoir age
MAR 05-04G	17	17	75	*Parvicardium exigum*	540 ± 50	155 ± 70	TO-13196
MAR 05-13P	16	46	75	Bivalve fragments	1380 ± 50	915 ± 60	TO-13198
MAR 05-13P	87	117	75	Bivalve fragments	2230 ± 60	1820 ± 75	TO-12906
MAR 05-04G	137	137	75	*Mytilus galloprovincialis*	2600 ± 60	2255 ± 80	TO-13197
MAR 05-13P	253	283	75	Bivalve fragments	3940 ± 60	3920 ± 90	TO-12907
MAR 05-13P	384	414	75	Bivalve fragments	4170 ± 60	4235 ± 90	TO-12908
MAR 05-13P	441	471	75	*Mytilus galloprovincialis*	4770 ± 70	5035 ± 110	TO-12909
MAR 05-13P	504	534	75	*Mytilus galloprovincialis*	5960 ± 80	6375 ± 85	TO-12910
MAR 05-13P	620	650	75	*Mytilus galloprovincialis*	6370 ± 90	6835 ± 115	TO-12911
MAR 05-13P	647	677	75	Bivalve fragments	7020 ± 100	7505 ± 90	TO-12912
MAR 05-13P	659	689	75	Just above alpha1	7310 ± 135	7805 ± 125	Extrapolation
MAR 05-13P	660	690	75	Just below alpha1	8280 ± 95	8940 ± 100	Extrapolation
MAR 05-13P	696	726	75	*Turricaspia spica*	8740 ± 70	9515 ± 75	TO-12834
MAR 05-13P	784	814	75	Bivalve fragments	9870 ± 90	10,915 ± 140	TO-12913
GeoB7625-2	46	46	1242	*Mytilus galloprovincialis* in GeoB7622-2	1170 ± 35	705 ± 35	KIA-25671
GeoB7625-2	158	158	1242	*Mytilus galloprovincialis* in GeoB7622-2	2095 ± 30	1660 ± 50	KIA-25749
GeoB7625-2	293	293	1242	*Mytilus galloprovincialis* in GeoB7622-2	2385 ± 35	2005 ± 55	KIA-25672
GeoB7625-2	388	388	1242	*Mytilus galloprovincialis* in GeoB7622-2	3080 ± 35	2840 ± 50	KIA-25751
GeoB7625-2	466	466	1242	Santorini ash		3331 ± 10	Friedrich et al., 2006
GeoB7625-2	538	538	1242	*Mytilus galloprovincialis* in GeoB7622-2	4605 ± 55	4805 ± 80	KIA-25674
GeoB7625-2	578	578	1242	organic matter in GeoB7622-2	5715 ± 25	6120 ± 50	KIA-19273
GeoB7625-2	614	614	1242	*Mytilus galloprovincialis* in GeoB7622-2	6590 ± 70	7090 ± 85	KIA-25675
GeoB7625-2	624	624	1242	*Mytilus galloprovincialis* in GeoB7622-2	7625 ± 55	7515 ± 50	KIA-25753
GeoB7625-2	639.5	639.5	1242	Gastropod in MD04-2760	8505 ± 45	8375 ± 50	KIA-26698
BC53	28.5	28.5	2153	End of transition sapropel	1635 ± 60	1180 ± 65	Jones and Gagnon, 1994
BC53	31	31	2153	First invasion of the coccolith *Emiliania huxleyi*	2720 ± 160	2430 ± 200	Jones and Gagnon, 1994

level of the Marmara Sea and the world ocean reached the Bosphorus sill depth. This one-way outflow was followed, after an initial short-lived pulse of saline inflow at ~9.14 cal ka BP, by two-way flow and progressive, gradual filling of the Black Sea after ~7.5 ^{14}C ka BP (here calibrated by us to ~8.0 cal ka BP) when the Bosphorus sill was sufficiently inundated that water could flow unimpeded in both directions (Mudie et al., 2007; Hiscott et al., 2007a,b). Marret et al. (2009), using the same Black Sea core as Hiscott et al. (2007b), proposed a gradual two-step filling of the Black Sea during the Holocene. Other paleosalinity studies have measured interstitial sediment water chlorinity and δ^{18}O values and concluded that freshwater (~1 psu) filled the Black Sea to at least −350 m until ca 9.0 cal ka BP (Soulet et al., 2010), while benthic ostracod δ^{18}O values were used by Bahr et al. (2006) and Vidal et al. (2010) to record apparent decreases or increases in salinity following disconnection of the Black and Marmara seas during the Lateglacial – Holocene period. van der Meer et al. (2008) determined that alkenones show a freshening of the surface Black Sea water during the past 3000 years.

Here we tackle the problem of conflicting interpretations of the Holocene Black Sea paleosalinity record by investigating four AMS-dated sediment records of annual sea surface salinity (SSS) using changes in the process length of a dinoflagellate cyst *Lingulodinium machaerophorum* (Deflandre et Cookson 1955) Wall 1967 that are quantitatively calibrated to modern regional surface water conditions over the salinity range of 12.2–18.5 psu. Process length of *Lingulodinium machaeorophorum*, the cyst of the autotrophic dinoflagellate *Lingulodinium polyedrum* (Stein 1883) Dodge 1989, was initially qualitatively related to presumed salinity changes in the Black Sea by Wall et al. (1973) and subsequently used

semi-quantitatively in other regions (Dale, 1996; Matthiessen and Brenner, 1996; Nehring, 1997; Ellegaard, 2000; Brenner, 2005; Sorrell et al., 2006; Head, 2007; Marret et al., 2009) and the Black and Marmara seas (Mudie et al., 2001; Londeix et al., 2009; Marret et al., 2009). Kokinos and Anderson (1995) first demonstrated the occurrence of different biometrical groups of cysts of *L. polyedrum* in culture experiments. Experiments by Hallett (1999) revealed a linear relationship between average process length of this taxon and both salinity and temperature. This relationship was confirmed for *L. machaerophorum* from globally distributed surface sediments by Mertens et al. (2009a). This proxy was applied to downcore salinity reconstructions in the Black Sea (Mudie et al., 2009; Verleye et al., 2009) and the Cariaco Basin (Mertens et al., 2009b). Early studies of dinoflagellate cysts showed they are abundant and diverse in Black Sea sediments and useful as paleoceanographical indicators (Wall and Dale, 1973, 1974; Wall et al., 1973); subsequently they have been applied in several more detailed regional studies (e.g. Mudie et al., 2001, 2002, 2004, 2007; Marret et al., 2009; Verleye et al., 2009). *L. machaerophorum* is continuously present in Black Sea sediments after the Holocene reconnection with the Mediterranean Sea, but has also been recorded earlier (Marret et al., 2009).

In this paper, we report on a new study of morphological variation of processes in *L. machaerophorum* extracted from 65 surface sediment samples from the Black Sea, Azov Sea and Caspian Sea (Fig. 1). These measurements are then calibrated against salinity data (Fig. 6) and this regional calibration is then used to reconstruct Holocene annual surface salinity changes in the Black Sea by stacking measurements downcore from a set of well-dated cores (Figs. 4 and 7). To validate the taxonomic integrity of this paleosalinity proxy, we also report the first results of molecular studies showing that SSU, LSU and ITS sequences of *L. machaerophorum* from the Black Sea and Caspian Sea are identical, and are the same as sequences in cultures established from *L. machaerophorum* from San Pedro Harbor, Southern California.

2. Environmental setting

The Black Sea is the largest anoxic marine basin in the world. It is connected to the Marmara Sea via the Strait of Bosphorus, which in turn is connected by the Dardanelles Strait to the Aegean and the Mediterranean seas (Figs. 1 and 2). The abyssal plain covers more than 60% of the total submerged area, and the average depth is 1240 m (Ross and Degens, 1974). The large continental shelf in the northwestern Black Sea narrows in a southerly direction. The circulation of the surface waters in the Black Sea is dominated by western and eastern gyres, which cover virtually the entire basin (Stanev, 2005). The narrow Rim Current flows counterclockwise and encloses both gyres. Anticyclonic eddies are present along the coast (Oğuz et al., 1993). Offshore, three distinct water masses are distinguished. These are a low salinity (mean annual value 17–20 psu), well-ventilated surface water mass occupying the upper 50–90 m of the water column, a suboxic cold intermediate water mass from 90 m to about 150 m, and a more saline, anoxic water mass below approximately 150 m (Murray, 1991). The oxic–anoxic boundary can change by several tens of meters diurnally and in a few years (Murray et al., 1989; Sorokin, 2002). The salinity of the upper water mass is almost half that of the Mediterranean Sea because of high river discharge and the restricted oceanic connection (Beşiktepe et al., 1994). The relatively low present day Black Sea sea surface salinity (SSS) (Fig. 2) is positively influenced by the Bosphorus bottom water inflow (ca 39 psu), and decreases away from the point of inflow due to an excess of precipitation and river inflow over evaporation (Beşiktepe et al., 1994; Kara et al., 2008). The water exchange between the Black Sea and Marmara Sea occurs as a two-layer flow in the Strait of Bosphorus (Latif et al., 1992). The cooler (5–15 °C) and less saline surface water mass from the Black Sea flows southwestward (Özsoy et al., 1995; Polat and Tuğrul, 1996), and forms a 25–100 m thick surface layer in the Marmara Sea and Aegean Sea (Beşiktepe et al., 1994). The bottom current in the Bosphorus is warmer (15–20 °C)

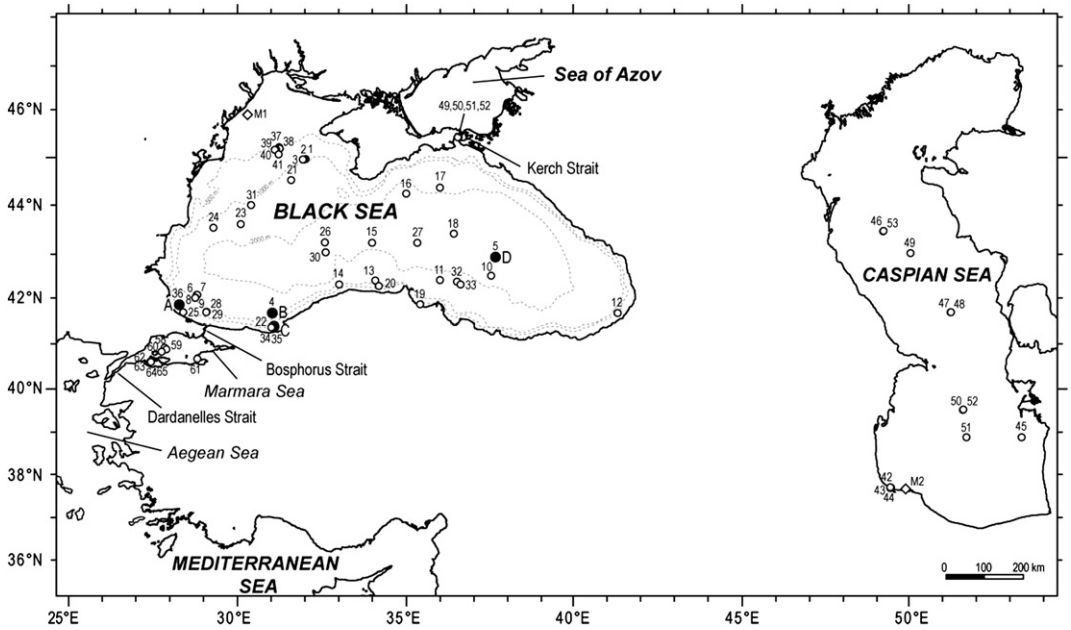

Fig. 1. Location map, showing the main geographic regions, the distribution of surface samples for morphological study (1–65) (indicated by empty circles) and molecular analysis (M1–M2) (indicated by diamonds) and position of the cores at the four core sites (indicated by filled circles) with corresponding numbers shown in Table 2 and Table 3. The four core sites are: A. Trigger-weight core MAR 02-45TWC and piston core MAR02-45P are from the same location on the Turkish Shelf northwest of the Bosphorus Strait. B. Gravity core GeoB7625-2 was recovered northeast of Sakarya River. C. Gravity core MAR05-4G and piston core MAR05-13P were recovered from the same site east of the Strait of Bosphorus. D. Boxcore BC53 was recovered in the deep Eastern Basin of the Black Sea.

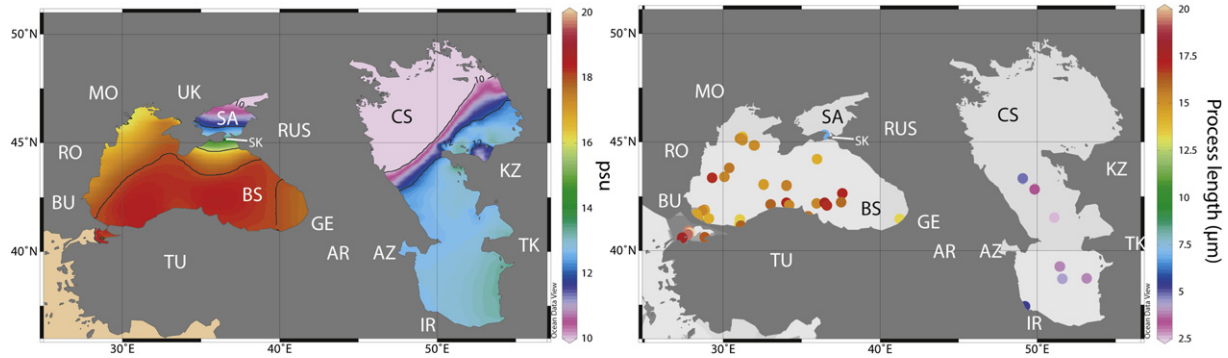

Fig. 2. Maps of surface salinity and process length distributions. A. Annual salinity in the Black Sea – Caspian Sea. B. Distribution of studied surface sediment samples, indicating average process lengths (µm) of *Lingulodinium machaerophorum*, major countries in the region (BU–UK), and the Black Sea (BS) connected to the Sea of Azov (SA) via the Kerch Strait (SK), and the Caspian Sea (CS). AR = Armenia, AZ = Azerbaijan, BU = Bulgaria, GE = Georgia, IR = Iran, KZ = Kazakhstan, MO = Moldova, RO = Romania, RUS = Russia, TK = Turkmenistan, TU = Turkey, UK = Ukraine.

and consists of a more saline (38–39 psu) mixture of Marmara Sea and Aegean Sea water (Özsoy et al., 1995; Polat and Tuğrul, 1996). This denser water flows northeastwards, cools on the southwestern Black Sea shelf, is diluted by mixing with the cold intermediate water layer, and sinks below the pycnocline toward the abyssal plain (Özsoy et al., 1995) where the bottom salinity is 22–24 psu.

The Kerch Strait connects the Black Sea and Azov Sea. This narrow and shallow (2.5 km wide, maximum 15 m deep) strait has a length of 48 km and covers an area of about 805 km^2. The flow of low salinity water from the Sea of Azov dominates in the Kerch Strait (Eremeev et al., 2003). The Kerch Strait salinity is ~12.5 psu (Il'in et al., 2001; Matishov et al., 2003).

The Caspian Sea is the world's largest inland sea in terms of both area and volume, stretching from 36°N to 62°N (Fig. 1). It has a drainage basin covering about 3.5 million km^2 (UNEP, 2006), compared to 2.4 million km^2 for the Black Sea. Water inputs comprise river discharges, including the Volga (contributing up to 80–85% of the total), Emba, Ural and Terek rivers (Rodionov, 1994). There is a north–south gradient in water salinity, with freshwater in the northern end of the basin to almost homogeneous water-column salinity (12.5–13.5 psu) in the central and southern basins (Kosarev and Yablonskaya, 1994). In the southern basin, seasonal salinity changes are less than ~0.2–0.4 psu. Mean annual salinity increases from the surface to the bottom waters only by 0.1–0.3 psu (Zenkevitch, 1963; Kosarev and Yablonskaya, 1994).

3. Material and methods

3.1. Location of surface samples and cores used for morphological measurements

Measurements of *L. machaerophorum* for 43 surface samples from the Black Sea, Marmara Sea and Caspian Sea were previously published by Mertens et al. (2009a). A total of 22 new surface sediment samples from the northeastern part of the Kerch Strait (Sea of Azov) (4), Black Sea (10), Marmara Sea (5) and Caspian Sea (3) were studied for biometric measurements of *L. machaerophorum* (Fig. 2B). For 20 of the 65 samples, the dinoflagellate cyst assemblages have been described in earlier papers (Marret et al., 2004, 2009; Mudie et al., 2004, 2007; Leroy et al., 2006; Verleye et al., 2009; Mertens et al., 2009a). Most were core-top samples from areas with relatively high sedimentation rates and can be considered recent, i.e. less than tens of years to a few centuries old (Table 2). It is assumed here that the environmental conditions affecting the morphological changes within the cysts are similar to recent environmental conditions.

Using the same method, morphological measurements were also obtained downcore for dinoflagellate cysts extracted from three short cores (MAR02-45TWC, MAR05-4G, BC53) and three longer piston (P) or giant gravity cores (MAR02-45P, MAR05-13P, GeoB7625-2), recovered from four core sites (Fig. 1). For the first site, trigger-weight core MAR02-45TWC and piston core MAR02-45P are from the same location on the SW Black Sea shelf northwest of Strait of Bosphorus. For the second site, GeoB7625-2, located northeast of Sakarya River, process length measurements have already been published (Verleye et al., 2009). For the third site, both gravity core MAR05-4G and piston core MAR05-13P were recovered from the same location east of Strait of Bosphorus. The fourth site is in the deep Eastern Basin of the Black Sea where core BC53 was recovered.

3.2. Chronology

All of these cores except core BC53 and GeoB7625-2 have been dated by multiple AMS radiocarbon ages on mollusks (Table 1) and the two sets of MAR cores complement each other in that, together, they cover the entire early Holocene to recent time interval. Core GeoB7625-2 was dated by correlation to the mollusk-based age model of nearby cores by Lamy et al. (2006) and Kwiecien et al. (2008). Core BC53 was dated by the radiocarbon dates of the first invasion of the coccolith *Emiliania huxleyi* (van der Meer et al., 2008). The age model and further sedimentological details for MAR02-45P and MAR02-45TWC are discussed in Hiscott et al. (2007b, 2010) and partly in Marret et al. (2009).

Raw radiocarbon ages (with units ^{14}C yr BP or ^{14}C ka) were converted to calendar years (with units cal yr BP or cal ka) using Oxcal4.0 online software, developed by the Oxford Radiocarbon Accelerator Unit (ORAU) and the Marine09.14c calibration curve. We use a reservoir age of 415 yr (Siani et al., 2000) for all raw dates younger than 7.1 ^{14}C ka. We use a reservoir age of 300 yr for all raw dates older than 8.4 ^{14}C ka in shelf cores MAR02-45, MAR05-04G and MAR05-13P, consistent with Soulet et al. (2011). 7.1 ^{14}C ka and 8.4 ^{14}C ka are, respectively, the times of euryhaline mollusk appearance and first influence of Mediterranean water identified by Ryan et al. (1997) and Ryan et al. (2003). For raw shell dates between 7.1 ^{14}C ka and 8.4 ^{14}C ka in shelf cores, we use linear interpolation to obtain an appropriate reservoir age between 300 yr and 415 yr. For our two deep-water sites, we use a reservoir age of 1000 yr prior to 7.5 ^{14}C ka and 415 yr for younger raw dates. Prior to 7.1–7.5 ^{14}C ka, the reservoir values are different for shelf sites and deep-water sites because

Table 2
Details of the locations, water depths, sampling device, estimated ages, morphological measurements and summer salinity (psu). A '*' denotes samples that were excluded.

Nr.	Region	Station	Reference	Latitude (°N)	Longitude (°E)	Water depth (m)	Core type	Estimated age (cal yrs)	Sed. rate (cm/ka)	% *L. mach.*	*L. mach.* process length (μm)	*L. mach.* body diameter (μm)	Specimens measured	Summer salinity (psu)
1	Black Sea	GC27	Mertens et al., 2009a	44.838	32.020	95	Gravity core	Recent	?	43.45	14.54	48.27	50	17.26
2	Black Sea	GC49	Mertens et al., 2009a	44.851	31.987	79	Gravity core	Recent	?	67.09	15.30	47.79	50	17.24
3	Black Sea	GC29	Mertens et al., 2009a	44.835	31.984	92	Gravity core	Recent	?	51.83	15.11	47.57	50	17.24
4	Black Sea	GeoB7625-2	Verleye et al., 2009	41.440	31.067	1242	Gravity core	255	112	52.00	13.36	43.69	100	18.55
5	Black Sea	BC53 core	Mertens et al., 2009a	42.651	37.601	2154	Boxcore	Recent	17	10.13	16.98	48.35	50	18.48
6	Black Sea	KNORR134-8,1 (GGC1)	Mertens et al., 2009a	41.889	28.820	549	Giant gravity core	Recent	?		15.50	48.27	50	17.68
7	Black Sea	KNORR134-8,2 (BC2)	Mertens et al., 2009a	41.865	28.835	660	Boxcore	Recent	?		14.49	46.16	50	17.69
8	Black Sea	KNORR134-8,6 (GGC4)	Mertens et al., 2009a	41.839	28.687	211	Giant gravity core	Recent	?		16.23	47.27	50	17.62
9	Black Sea	KNORR134-8,11 (GGC7)	Mertens et al., 2009a	41.836	28.690	208	Giant gravity core	Recent	?		15.31	48.20	50	17.62
10	Black Sea	KNORR134-8,70 (GGC35)	Mertens et al., 2009a	42.250	37.527	2060	Giant gravity core	Recent	?		15.92	47.10	50	18.41
11	Black Sea	KNORR134-8124 (GGC64)	Mertens et al., 2009a	42.193	35.983	203	Giant gravity core	Recent	?		15.29	46.02	50	18.69
12	Black Sea	KNORR134-8101 (GGC51)	Mertens et al., 2009a	41.471	41.257	1406	Giant gravity core	Recent	?		13.30	46.84	35	17.67
13	Black Sea	KNORR134-8150 (GGC72)	Mertens et al., 2009a	42.207	34.054	435	Giant gravity core	Recent	?		17.39	46.66	30	18.32
14	Black Sea	AII 1431	Mertens et al., 2009a	42.233	33.067	2136	Piston core	Recent	?		16.13	47.27	50	18.24
15	Black Sea	AII 1432	Mertens et al., 2009a	43.010	34.075	2248	Gravity core	Recent	?		15.41	45.64	50	18.54
16	Black Sea	AII 1433*	Mertens et al., 2009a	44.083	35.000	2225	Trip gravity core	Recent	?		10.96	44.08	50	18.16
17	Black Sea	AII 1434	Mertens et al., 2009a	44.333	36.000	1466	Gravity core	Recent	?		14.25	44.94	50	17.76
18	Black Sea	AII 1436*	Mertens et al., 2009a	43.400	36.600	2158	Trip gravity core	Recent	?		11.74	43.52	50	18.72
19	Black Sea	AII 1438	Mertens et al., 2009a	41.975	35.683	284	Gravity core	Recent	?		15.84	46.45	50	18.20
20	Black Sea	AII 1440	Mertens et al., 2009a	42.203	34.355	264	Piston core	Recent	?		15.30	45.85	50	18.33
21	Black Sea	AII 1443*	Mertens et al., 2009a	44.587	31.922	1057	Trip gravity core	Recent	?		12.33	43.59	50	17.45
22	Black Sea	AII 1447	Mertens et al., 2009a	41.383	31.062	1256	Piston core	Recent	?		13.25	45.14	50	18.54
23	Black Sea	AII 1450	Mertens et al., 2009a	43.657	30.157	563	Gravity core	Recent	?		15.27	46.24	50	17.68
24	Black Sea	AII 1451	Mertens et al., 2009a	43.570	29.525	460	Gravity core	Recent	?		16.94	46.37	50	17.14
25	Black Sea	AII 1453	Mertens et al., 2009a	41.843	28.687	255	Gravity core	Recent	?		14.51	44.24	50	17.61
26	Black Sea	AII 1462 Z4B	Mertens et al., 2009a	43.075	32.992	2179	Kasten core	Recent	?		14.69	46.26	42	18.30
27	Black Sea	AII 1464*	Mertens et al., 2009a	43.032	35.478	2173	Kasten core	Recent	?		11.39	43.27	50	18.86
28	Black Sea	B2KS01 0-1	Mertens et al., 2009a	41.491	29.122	88.8	Kullenberg	Recent	?		14.69	47.36	50	17.82
29	Black Sea	B2KS02 0-1	Mertens et al., 2009a	41.491	29.122	88.8	Kullenberg	Recent	?		14.20	47.67	50	17.82
30	Black Sea	B2KS33 0-1*	Mertens et al., 2009a	42.838	32.593	2173	Kullenberg	Recent	?		12.27	45.70	50	18.34
31	Black Sea	B2KS38 0-1	Mertens et al., 2009a	43.804	30.401	355	Kullenberg	Recent	?		15.69	47.34	50	17.46
32	Black Sea	Core 22-MUC-1	Unpublished	42.222	36.489	842	Multi-corer	Recent	31.25	63.23	17.68	48.81	50	18.64
33	Black Sea	Core 25-MUC-2	Unpublished	42.102	36.621	418	Multi-corer	Recent	31.25	8.41	16.86	53.80	50	18.58
34	Black Sea	M05-4G	Unpublished	41.166	31.129	75	Gravity core	Recent	32		15.49		44	18.57
35	Black Sea	MAR05-13P 30 cm	Unpublished	41.166	31.128	75	Piston core	900	32	82.00	16.03	48.88	50	18.57
36	Black Sea	MAR02-45TWC 10 cm	Unpublished	41.685	28.317	10	Trigger weight core	80	1000	85.19	14.45		50	17.52
37	Black Sea	SH1	Unpublished	45.243	31.222	25	Boxcore	Recent	?		13.48	45.53	50	16.36
38	Black Sea	SH3	Unpublished	45.186	31.249	50	Boxcore	Recent	?		14.35	43.27	50	16.44
39	Black Sea	SH4	Unpublished	45.154	31.135	50	Boxcore	Recent	?		14.46	45.07	50	16.41
40	Black Sea	SH5	Unpublished	45.150	31.078	49	Boxcore	Recent	?		15.22	44.74	50	16.37
41	Black Sea	SH7	Unpublished	45.094	31.229	51	Boxcore	Recent	?		15.21	43.76	50	16.51
42	Caspian Sea	Enseli Lake 1	Unpublished	37.400	49.450	2.5	PVC Tube	Recent	?	11.72	4.46	57.44	50	12.63
43	Caspian Sea	Enseli Lake 2	Unpublished	37.400	49.450	2.5	PVC Tube	Recent	?	11.72	5.23	53.88	8	12.63
44	Caspian Sea	Enseli Lake 4	Unpublished	37.410	49.447	2.5	PVC Tube	Recent	?	11.72	4.59	67.13	50	12.63
45	Caspian Sea	US09	Marret et al., 2004	38.734	53.185	13	Usnel boxcore	Recent	?	43.50	3.82	46.20	50	12.83
46	Caspian Sea	US26	Marret et al., 2004	43.323	49.093	61	Usnel boxcore	Recent	?	21.60	4.11	47.74	50	11.90
47	Caspian Sea	CP18	Marret et al., 2004	41.539	51.100	480	Pilot	Mid-Holocene	?	5.90	4.10	53.63	8	12.51
48	Caspian Sea	GS18	Marret et al., 2004	41.542	51.101	480	Kullenberg	Mid-Holocene	?	33.00	2.64	47.10	24	12.51
49	Caspian Sea	CP21	Marret et al., 2004	42.839	49.853	460	Pilot	Mid-Holocene	?	5.20	3.40	47.29	7	12.29
50	Caspian Sea	CP14	Marret et al., 2004	39.270	51.458	315	Pilot	809	35	7.00	3.38	50.18	11	12.74
51	Caspian Sea	CP04	Marret et al., 2004	38.722	51.606	405	Pilot	Holocene	?	13.19	4.38	50.58	50	12.81
52	Caspian Sea	US02	Marret et al., 2004	39.267	51.483	315	Usnel boxcore	Recent	?	10.84	3.81	57.20	14	12.73
53	Caspian Sea	US24	Marret et al., 2004	43.318	49.100	61	Usnel boxcore	Recent	?	6.70	4.75	50.00	50	11.90

(*continued on next page*)

Table 2 (*continued*)

Nr.	Region	Station	Reference	Latitude (°N)	Longitude (°E)	Water depth (m)	Core type	Estimated age (cal yrs)	Sed. rate (cm/ka)	% *L. mach.*	*L. mach.* process length (μm)	*L. mach.* body diameter (μm)	Specimens measured	Summer salinity (psu)
54	Sea of Azov	N4	Unpublished	45.339	36.472	3.5	Pushcore	Recent	?		6.76	48.47	50	13.09
55	Sea of Azov	N14	Unpublished	45.339	36.472	5	Pushcore	Recent	?		6.90	46.25	50	13.09
56	Sea of Azov	N18	Unpublished	45.339	36.472	1.5	Pushcore	Recent	?		7.20	48.95	50	13.09
57	Sea of Azov	N22	Unpublished	45.339	36.472	3	Pushcore	Recent	?		7.06	46.58	50	13.09
58	Marmara Sea	DM5	Caner and Algan, 2002	40.921	27.825	645	Gravity core	Recent	10–23		19.47	46.49	50	21.57
59	Marmara Sea	DM18	Caner and Algan, 2002	40.831	27.877	895	Gravity core	Recent	10–23		20.10	46.23	34	21.74
60	Marmara Sea	DM13	Cagatay et al., 2000	40.761	27.751	709	Gravity core	Recent	10–23		19.26	46.37	39	21.88
61	Marmara Sea	MAR02-88P	Unpublished	40.627	28.842	340	Gravity core	Recent	?		16.19	43.80	52	20.83
62	Marmara Sea	MAR02-012	Unpublished	40.568	27.392	69.5	Van Veen grab	Recent	?		18.32	45.92	40	22.17
63	Marmara Sea	MAR02-013	Unpublished	40.573	27.402	74	Van Veen grab	Recent	?		19.20	46.85	22	22.17
64	Marmara Sea	MAR02-014	Unpublished	40.588	27.404	79.4	Van Veen grab	Recent	?		18.29	46.22	50	22.17
65	Marmara Sea	MAR02-018	Unpublished	40.625	27.409	110.1	Van Veen grab	Recent	?		17.84	45.57	24	22.13

of water-column stratification (Kwiecien et al., 2008). Extrapolated ages on either side of unconformities α_1 and α_2 have error bars consistent with all combinations of ±errors of the two radiocarbon ages above and below that level. Radiocarbon dates for core GeoB7625-2 were calibrated by Lamy et al. (2006) using a reservoir age of 475 years. To be consistent with other calibrations in this paper, we have recalibrated the Lamy et al. (2006) dates using parameters specified above and in the Table 1 caption, and show these results in Table 1.

The dates show that, in core MAR02-45P, there is a ~3.41 cal ka hiatus between 161 and 160 cm (non-deposition from 5.46 to 2.05 cal ka BP) and in MAR05-13P, there is a ~1.14 cal ka hiatus between 660 and 659 cm (non-deposition from 8.94 to 7.80 cal ka BP). The age model also shows that in MAR02-45P and MAR02-45TWC, the sampling intervals are ~0.238 cal ka and ~0.185 cal ka respectively. For GeoB7625-2 the sampling interval is ~0.228 cal ka (Verleye et al., 2009) and for BC53, the sampling interval is ~0.300 cal ka (van der Meer et al., 2008). In cores MAR05-4G and MAR05-13P, the sampling intervals are ~0.164 cal ka and ~0.214 cal ka respectively (Cranshaw, 2007).

3.3. Palynological preparation and light microscopy

All the cysts were extracted from the sediments using methods described in the respective publications shown in Table 2. Most were standard palynological methods involving hydrochloric acid (HCl) and hydrofluoric acid (HF), sieving and/or sonification. For two surface samples (Core 22-MUC-1, Core 25-MUC-1), heavy liquid separation using sodium polytungstate with a density of 2.1 g ml^{-1} was used (Bolch, 1997). No acetolysis or potassium hydroxide (KOH) were utilized. Regardless of the extraction methods used for this study, comparison of cysts between different samples showed no differences in cyst preservation. This suggests that the different processing methods employed in this study had no effect on measurements of *L. machaerophorum*, as noted previously by Mertens et al. (2009a, 2010).

All measurements were made using a Zeiss Axioskop 2 equipped with an AxioCam MRc5 digital camera (Axiovision v. 4.6 software), Nikon Eclipse80i, Nikon E400 light microscope or an Olympus BH-2 light microscope equipped with Color View II (Cell F Software Imaging System) and 63×–100× objectives. All measurements were made by K. N. Mertens, L. R. Bradley, P. Mudie and T. Verleye. For each sample, the average of the length of the three longest visible processes and the largest body diameter of 50 cysts per sample were measured, if possible. Measuring 50 cysts yields reproducible results (Mertens et al., 2009a); like Head (2007) we found that average process length per sample for *L. machaerophorum* is reproducible within ~1 μm. The length of each process was measured from the middle of the process base to the process tip. It is important to note that no cysts without processes (i.e. "zero" process length) were included in the analysis, because of the difficulty of species identification associated with these forms and the desire to exclude observer bias from the measurements. For each cyst, three processes could always be found within the focal plane of the light microscope, so this number seemed a logical choice. There are three reasons for choosing the longest processes. 1. The longest processes reflect unobstructed growth of the cyst. 2. Measuring the longest processes increases accuracy because it documents the largest variation. 3. Since only a few processes were parallel to the focal plane of the microscope, it was imperative to make a consistent choice. Sometimes fewer than 50 cysts were measured, if more were not present. Fragments representing less than half of a cyst and cysts with mostly broken processes were not measured.

3.4. Salinity and temperature data

Biometric measurements on cysts from the surface samples in the Black Sea, Caspian Sea and Kerch Strait were compared to both seasonal and annual temperature (T), salinity (S), the ratio between salinity and temperature (S/T) and sea water density (D) at depths spanning the range 0–30 m using the gridded 1/4° World Ocean Atlas 2001 (Locarnini et al., 2002) and the Ocean Data View software (Schlitzer, 2010) by calculating Pearson's correlation coefficient. Because World Ocean Atlas 2001 yields anomalous data for the Marmara Sea, salinity and temperature data were obtained from MEDAR/MEDATLAS II (MEDAR Group, 2002) for the samples from Marmara Sea. The significance of Pearson's r was calculated using a t-test.

3.5. Molecular analysis

Three surface samples were collected from the Northwestern Black Sea (M1), southwestern Caspian Sea (M2) and San Pedro Harbor (M3) (California) (Table 3). Cysts were isolated from the sediment using heavy liquid separation using sodium polytungstate with a density of 1.3 g ml^{-1} (Bolch, 1997). We used cysts from the southwestern Caspian Sea and the Northwestern Black Sea, and germinated and cultured cells from San Pedro Harbor for molecular analyses. An isolated cyst was sonicated in a 200 μL PCR tube with sterilized seawater in order to remove extraneous matters. The cysts and the cells were individually transferred on a slide glass with a frame of vinyl tape, and observed and photographed using an Olympus BX51 microscope equipped with Nomarski differential interference contrast optics (Olympus, Tokyo, Japan) and with an Olympus DP71 digital camera. After taking photographs the cover slip was carefully removed. Under an inverted microscope (Olympus CKX41) the cell was picked up and crushed with a fine glass needle. The whole crushed cell was transferred into a 200 μL PCR tube containing 3 μL of Milli-Q water. This technique and the following PCR protocol are modifications of the methods in Takano and Horiguchi (2005). We determined sequences of ITS regions (internal transcribed spacer 1–5.8 rDNA - ITS2) and partial sequences of SSU and LSU rDNA from single-cysts and 5–10 cultured cells. In the first round of PCR, the external primers (SR1 and LSU R2; Takano and Horiguchi, 2005) were used with PCR mixtures of KOD-Plus-Ver. 2 Kit (Toyobo, Osaka, Japan) and the PCR conditions; one initial cycle of denaturation at 94 °C for 2 min, followed by 35 cycles of denaturation at 94 °C for 30 s, annealing at 50 °C for 30 s, and extension at 72 °C for 2 min and final extension at 72 °C for 5 min. In the second round of PCR, two sets of primers (SR12cF and 25R1, LSU D1R and LSU R2; Takano and Horiguchi, 2005) were used with PCR mixtures of KOD-Plus-Ver. 2 Kit (Toyobo, Osaka, Japan), 0.5 μL of the first round PCR product as DNA template, and the same PCR conditions except for extension at 72 °C for 1 min. In the third round of PCR, three sets of primers (SR12cF and 25F1R, LSU D1R and 25R1, LSU D3A and LSU R2; Takano and Horiguchi, 2005) were used with PCR mixtures of the TaKaRa EX taq system (Takara Bio Inc., Shiga, Japan), 0.5 μL of the second round PCR products as DNA template, and the same PCR conditions except for extension at 72 °C for 30 s. PCR products were sequenced directly using the ABI PRISM BigDye Terminator Cycle Sequencing Kit (Perkin–Elmer, Foster City, CA, USA). We sequenced both the forward and reverse strands. Obtained sequences were manually aligned.

Table 3
Details of the locations, water depths, sampling devices of samples used for molecular analysis.

Nr.	Region	Latitude (°N)	Longitude (°E)	Water depth (m)	Core type
M1	Black Sea	45.90	30.29	3.5	Pushcore (by diving)
M2	Caspian Sea	37.51	49.91	25	Van Veen Grab
M3	San Pedro Harbor (California)	33.74	−118.24	5	Petite Ponar Grab

4. Results

4.1. Process length variation in surface sediments and relation to environmental parameters

4.1.1. Overall cyst biometrics

Five surface samples from deeper parts of the Black Sea were excluded from the analysis because these samples had process lengths significantly shorter than comparable samples (AII 1433, AII 1436, AII 1443, AII 1464 and B2KS33 0-1) (Table 4, one-tailed t-test of unpaired samples with unequal variance, $p < 10^{-6}$). This is likely because the upper sedimentary section at these gravity-core sites was blown away during coring, resulting in morphologies in the top samples that are deemed unrepresentative of the actual surface. For the other surface samples, 8058 process length measurements were made. They gave an average of 13.4 μm with a standard deviation of 5.5 μm, and a range from 0.5 to 29.6 μm (Fig. 3A). Most cysts encountered were comparable to the forms described by Marret et al. (2004) for the Caspian Sea and by Wall et al. (1973), Mudie et al. (2001, 2004) and Marret et al. (2009) for the Black Sea. Cysts without processes were rarely observed but not measured. The range found is within the global range of 0–41 μm described by Mertens et al. (2009a). The skewness of the distribution was −0.43, because of the high number of short-process bearing cysts from the Caspian Sea in the sample population. If the size-frequency curves of the regions are observed separately, one easily sees that this curve is the sum of the separate unimodal curves of the Black Sea, Caspian Sea, Marmara Sea and the Kerch Strait (Sea of Azov), which only partly overlap and thus can clearly be distinguished from each other (Fig. 3B). The 2370 body diameter measurements average 47.6 μm with a standard deviation of 6.1 μm, over a range from 26 to 91 μm (Fig. 3C). This relatively large range can be explained partly by cysts sometimes being compressed or torn, resulting in an anomalously large body diameter (see also Mertens et al., 2009a). This mechanical deformation of the cyst also explains a positive skewness of the size-frequency spectrum (1.62). The Black Sea, Caspian Sea and the Kerch Strait all show similar size-frequency curves of body diameter when plotted separately (Fig. 3D).

4.1.2. Correlations between the environmental parameters and morphology

Pearson's correlation coefficient was calculated between average process length and S, T, S/T and D from 0 to 30 m, as reported both annually and seasonally (Table 5). There was a significant correlation

Table 4
Comparison between outliers and comparable samples using a one-tailed, t-test of unpaired samples with unequal variance. All probabilities are $<10^{-6}$, entailing a significant difference.

Outlier sample	Comparable sample →	AII 1432	AII 1434	AII 1438
	Average process length (μm) →	15.41	14.25	15.84
↓	↓			
AII 1433	10.96	1.67E-18	1.95E-13	6.18E-24
AII 1436	11.74	2.23E-14	2.03E-09	1.87E-19
AII 1443	12.33	2.39E-10	5.94E-06	2.86E-14
AII 1464	11.39	3.40E-17	4.60E-12	4.64E-23
B2KS33 0-1	12.27	3.34E-11	1.39E-06	1.47E-15

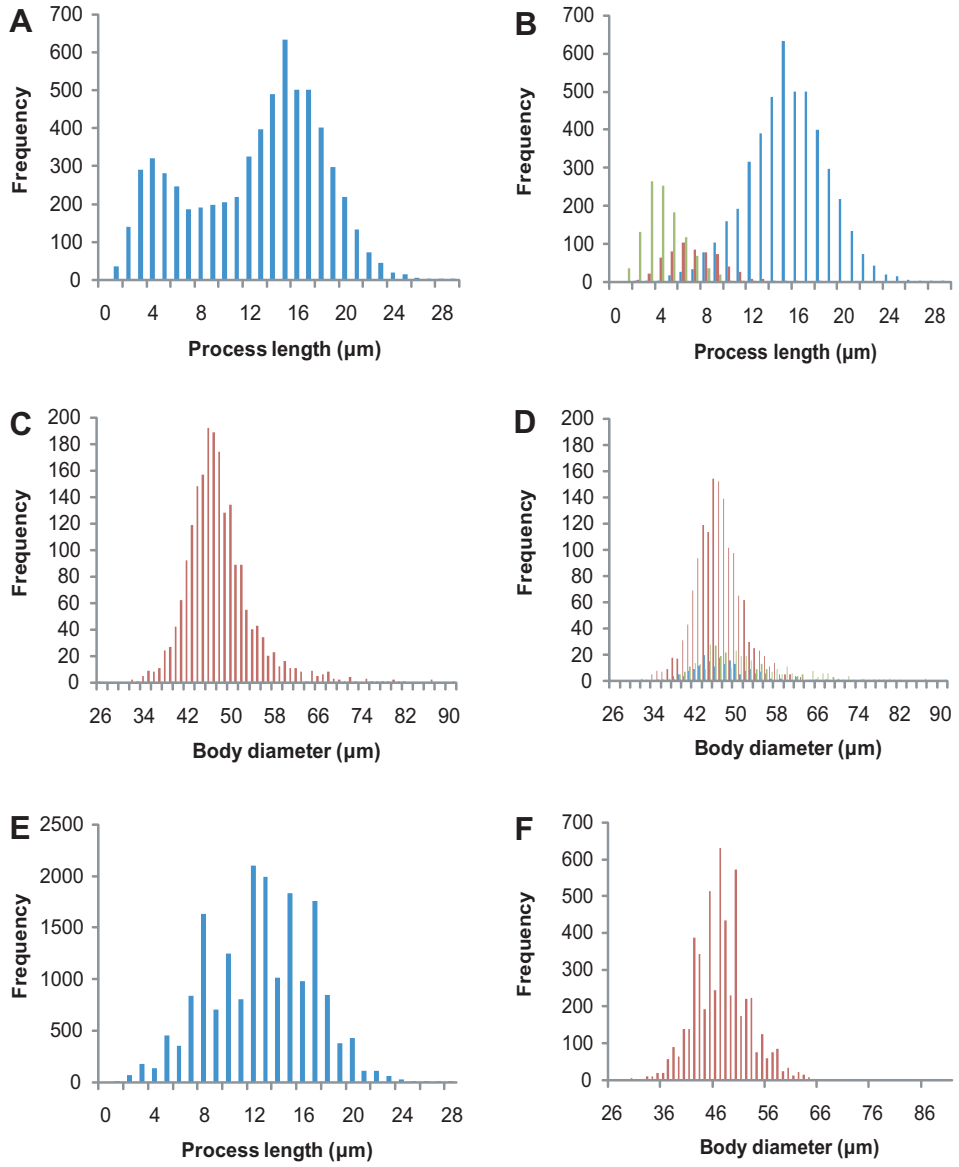

Fig. 3. Size–frequency spectra of process length and body diameter measurements of *Lingulodinium machaerophorum* in surface sediments (A–D) and downcore (E–F) in the Black Sea, Caspian Sea, and the Kerch Strait. Size–frequency spectra of 6375 process lengths for all measurements (A) and for Black Sea, the Kerch Strait and Caspian Sea separately (B) and of 2125 body diameter for all measurements (C) and for Black Sea, the Kerch Strait and Caspian Sea separately (D). Size–frequency spectrum of 18,117 process length measurements (E) and 5295 body diameter (F) measurements downcore for 6 cores from the Black Sea.

between process length and all parameters except for most of the temperatures ($p < 1 \times 10^{-16}$, Table 5). Correlation coefficients become less significant with depth for all parameters studied. The correlations of average process length to S, D and S/T are of similar significance on an annual and seasonal basis, except for winter where S/T is significantly less correlated.

No significant correlation was found between the process length and cyst body diameter ($R^2 = 0.25$). This confirms previous observations by Mertens et al. (2009a), as expected because culture experiments have failed to reveal any correlation between body diameter and salinity (Hallett, 1999). Variations in cyst body diameter are most likely caused by compression or formed during cyst germination. There was no significant correlation between water depth and average process length ($R^2 = 0.06$), and no significant correlation was found between relative abundance of *L. machaerophorum* and either average process length ($R^2 = 0.40$) or body diameter ($R^2 = 0.22$).

4.2. Downcore records of process length variation

4.2.1. Overall cyst biometrics

The 18,117 process length measurements obtained from core samples give a mean of 12.63 µm with a standard deviation of 4.1 µm, and a range from 1.0 to 28.4 µm (Fig. 3E). The range of cyst morphology is the same as described for the surface samples (Section 4.1.1). The observed downcore range of process length fits exactly within the global range of 0.5–28.9 µm measured in the surface sediments. The skewness of the distribution is −0.08, which makes the distribution effectively symmetrical. The 5295 maximum body diameter measurements give an average maximum body diameter of 47.3 µm with a standard deviation of 5.3 µm, over a range from 26 to 79 µm (Fig. 3F). This range is again comparable to the range of 26–91 µm measured in the surface sediments. There is no relation between process length and relative abundance (% *L. machaerophorum*) downcore ($R^2 = 0.0$).

Table 5
Pearson's correlation coefficient calculated between environmental parameters and average process length of *Lingulodinium machaerophorum* at water depths of 0 to 30 m. Significant correlations using the *t*-test ($p < 1 \times 10^{-12}$) are indicated in bold.

Parameter/Depth (m)	0	10	20	30
Annual T	0.03	0.12	0.24	0.02
Annual S	**0.81**	**0.76**	0.58	0.48
Annual S/T	**0.85**	**0.81**	0.64	**0.70**
Annual D	**0.84**	**0.79**	0.61	0.51
Summer T	0.01	0.30	0.43	0.25
Summer S	**0.88**	**0.86**	0.61	0.48
Summer S/T	**0.90**	**0.89**	0.63	**0.70**
Summer D	**0.90**	**0.90**	0.65	0.54
Autumn T	0.00	0.00	0.01	0.00
Autumn S	**0.79**	**0.74**	0.54	0.47
Autumn S/T	**0.78**	**0.70**	0.58	0.58
Autumn D	**0.82**	**0.75**	0.57	0.50
Winter T	0.00	0.01	0.00	0.05
Winter S	**0.73**	**0.70**	0.58	0.49
Winter S/T	0.20	0.22	0.07	0.01
Winter D	**0.74**	**0.71**	0.59	0.51
Spring T	0.06	0.17	0.46	0.01
Spring S	**0.84**	**0.79**	0.60	0.49
Spring S/T	**0.88**	**0.89**	**0.72**	**0.79**
Spring D	**0.89**	**0.84**	0.64	0.53

4.2.2. Process length variation downcore

Age models were used to assign measurements of process lengths to the time of deposition in calendar years BP. Significant downcore changes in process lengths of *L. machaerophorum* occur in the six studied cores (Fig. 4). Average process length varies between 17.6 and 14.2 μm in BC53, between 16.5 and 5.7 μm in GeoB7625-2, between 15.5 and 2.6 μm in cores MAR02-45P and MAR02-45TWC and between 16.7 and 8.2 μm in cores MAR05-3P and MAR05-4G.

After interpolating all the process lengths in all cores to a 10 calendar year time-step, we created a regional average process length record by calculating a weighted average from all interpolated values, using the number of specimens measured per core as weight. This resulted in a regional record ranging from 9.9 to 0.00 cal ka BP (Fig. 4). The standard deviation of the regional average is calculated by taking the square root of the sum of squares of the interpolated standard deviations divided by the number of standard deviations. The calculated average shows a very gradual increase in process length from 9.1 to 15.7 μm between 9.9 and 0.0 cal ka BP. There is a small dip between 7.7 and 7.3 cal ka BP. Because less than 50 specimens were found between 9.9 and 7.5 cal ka BP, there is more scatter in the regional average for this particular time slice (Fig. 4).

4.3. Molecular analysis

We determined sequences of SSU (1730 bp), ITS regions (535 bp) and partial LSU rDNA (1324 bp) from one single-cyst from the Northwestern Black Sea (SSU; AB693195, ITS; AB678399, LSU; AB678400), six single-cysts from the southwestern Caspian Sea (SSU; AB693194, ITS; AB678401, LSU; AB678402) and four strains established from cysts from San Pedro Harbor (SSU; AB693196, ITS; AB678403, LSU; AB678404). One of the sequenced cysts from each locality is shown in Fig. 5. Comparisons of the obtained sequences from the three localities shows that they are identical except for one degenerate site, Y (T and C) in the 1730 bp SSU from the Northwestern Black Sea and the southwestern Caspian Sea which was consistently T at the site from San Pedro Harbor. This confirms that all studied cysts, modern Caspian short process bearing and Black Sea and Californian longer process bearing cyst morphotypes of *L. machaerophorum* belong to the same species and that strain-specific responses are not a plausible factor in process length.

5. Discussion

5.1. Construction of salinity proxy and influence of temperature

Both salinity and temperature have been suggested to cause morphological variations of *L. machaeorophorum* in laboratory

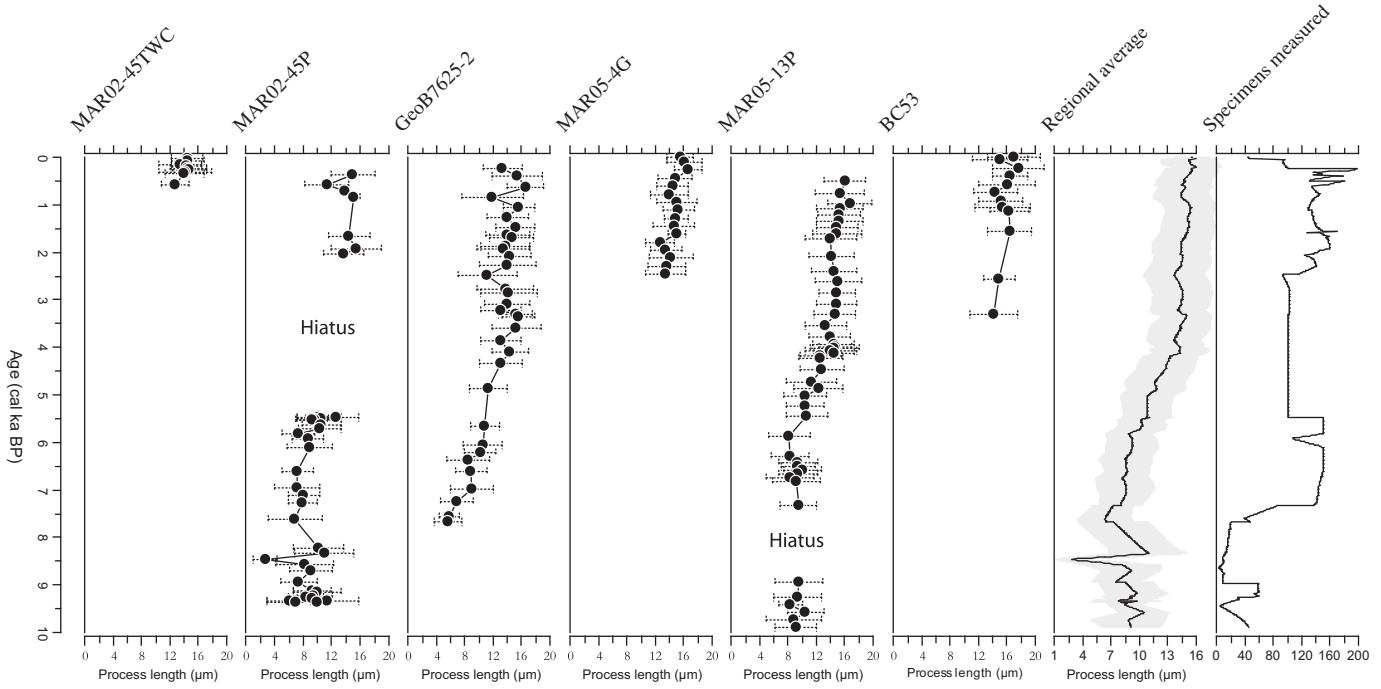

Fig. 4. Average process length variation of *Lingulodinium machaerophorum* in cores MAR02-45P and MAR02-45TWC (core site 1), GeoB7625-2 (core site 2), MAR05-13P and MAR05-4G (core site 3) and BC53 (core site 4), regional average and number of specimens measured. The regional average is calculated by averaging the interpolated values at a time-step of 10 years. All graphs are plotted against calendar age (cal ka BP). The error bars on the process lengths represent ±1 standard deviation.

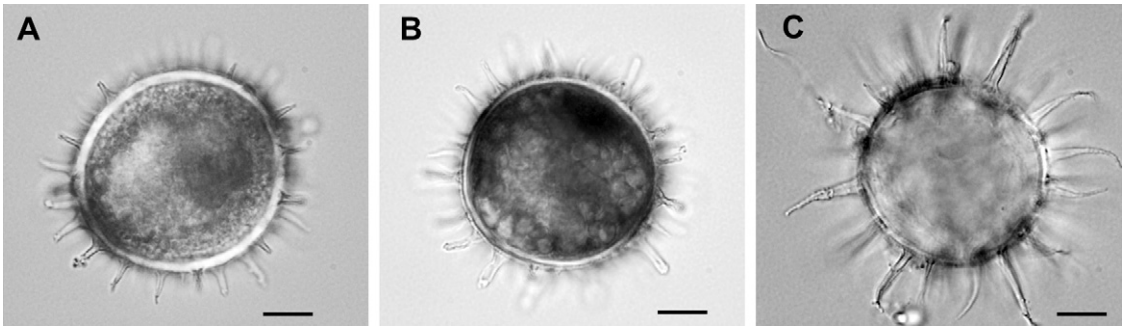

Fig. 5. Examples of cysts that were sequenced from the three study areas, which had identical SSU (1730 bp), ITS regions (535 bp) and partial LSU rDNA (1368 bp). A. Short process bearing cyst from southwestern Caspian Sea. B. Longer process bearing cyst from northwestern Black Sea. C. Very long process bearing cyst that germinated from San Pedro Harbor, California and where the cell was sequenced. All scale bars are 10 μm.

cultures (Hallett, 1999) and in the field (Mertens et al., 2009a). However, the Pearson's correlation coefficients show no direct linear relation between process length and temperature in the regional process length variation of cysts from surface sediments (Table 5). It is possible, however, that the influence of temperature is reflected in the calculated densities, which show similar correlation coefficients to those for salinity, both annually and seasonally. The covariation of salinity and density in the study region makes it impossible to disentangle the influence of both parameters. Pearson's correlation coefficients between sea surface salinity and sea surface density are high, both annually and seasonally ($R^2 > 0.97$). This correlation is similar for conditions deeper in the water column, i.e. at 10, 20 and 30 m. Thus, from our data alone we cannot determine unequivocally whether salinity or density is the most important factor in causing changes in process length. Extending this research to other regions where salinity and density do not covary could resolve this issue. Nevertheless, we consider it safe to assume that our proxy can be used for reconstruction of sea surface salinity (SSS) in the Black Sea, Marmara Sea and Caspian Sea, since both density and salinity which give the more significant correlations, are highly correlated in this region. The process length variations are a summer signal because *L. polyedrum* predominantly occurs during summer in the Black Sea (e.g. Türkoğlu and Koray, 2002), Marmara Sea (e.g. Balkis, 2003) and Caspian Sea (e.g. Bagheri et al., 2010).

A two degree polynomial between average process length (PL) and summer salinity (SSS_{summer}) provides a more significant correlation than a simple linear regression line ($R^2 = 0.91$ compared to 0.88). For our study region, therefore, we provide the following equation (Fig. 5): $SSS_{summer} = 0.026^{*}PL^2 - 0.0145PL + 12.136$ ($R^2 = 0.91$). Such a polynomial relation is not surprising, since the relation to process length has been suggested to be unimodal for *L. machaerophorum* (Hallett, 1999). The standard error on the reconstructed SSS_{summer} is 0.91 psu. For the Black Sea, this equation can be used at least to reconstruct salinities between 11.9 and 22.2 psu, which is the range of our measured samples.

Although it might seem that the process length–salinity relation merely connects four large clusters that could be separate populations (Fig. 6), we consider this incorrect for several reasons. One reason is that culture experiments using monoclonal strains of *L. polyedrum* show a unimodal relation of average process length to salinity over a broad range of salinities and process lengths (Lewis and Hallett, 1997; Hallett, 1999). Furthermore, a closely related species, *Protoceratium reticulatum*, also shows a significant ($R^2 = 0.8$) linear relation to salinity (and density) in the Baltic-Kattegat-Skaggerak estuarine system (Mertens et al., 2010). In addition, the molecular analysis shows that all studied sequences are identical, confirming that all examined cysts belong to the same species and that strain-specific responses are not a plausible factor in process length. This confirms morphological observations since the motile stage has been identified in the plankton as *L. polyedrum* in the Black Sea (e.g. Türkoğlu and Koray, 2002), Marmara Sea (e.g. Balkis, 2003) and Caspian Sea (e.g. Bagheri et al., 2010) and the cyst in the sediment as *L. machaerophorum* in the Black Sea (e.g. Wall et al., 1973), Marmara Sea (e.g. Londeix et al., 2009) and Caspian Sea (Marret et al., 2004). However, the morphological clusters in Fig. 6 individually do not show a significant linear relation to salinity within the Caspian Sea, Marmara Sea, Kerch Strait or Black Sea. This may be because of lateral transport of cysts within the individual sample areas which could mix the individual salinity responses and cause an overrepresentation of the most widespread morphotypes, particularly in areas with low sedimentation rates. Although this mixing reduces the precision for reconstruction of local salinities, averaging for reconstruction of regional signals as done here is warranted (see Section 5.3). Furthermore, these results significantly extend the geographic range of previous SSU and ITS rDNA studies (e.g. Frommlet and Eglesias-Rodriguez, 2008) that have previously shown the molecular identity of *L. machaerophorum* from Swedish (Koljö Fjord) and Californian populations.

5.2. Downcore variability: synchronous and diachronous changes in process length

There are observed differences between the 4 core sites depicted in Fig. 4 in the amplitude of change in process length, but not in the rates of change in process length. In terms of amplitude, it is

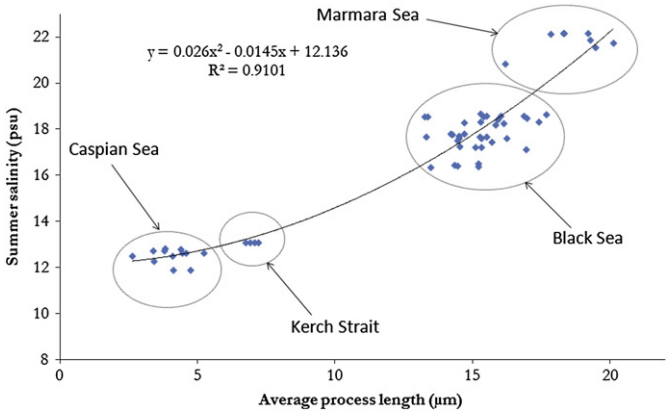

Fig. 6. Relationship between average process length of *Lingulodinium machaerophorum* and annual sea surface salinity (SSS). The linear trendline is a least squares fit to the three main clusters of samples from the Caspian Sea, Black Sea and the Kerch Strait. The equation for the regression line is given.

remarkable that the cores show distinct differences in process length during certain time-slices. For instance, around 8.5 cal ka BP there is a distinct drop in process length in one sample from core MAR02-45P (closest to the vast Danube-Dneister river drainage). There is no doubt that such differences can be related to local salinity effects, where lowered salinity briefly resulted in reduced process lengths. A similar local reduction in process length has been documented for the Berre coastal lagoon in the Mediterranean, where it has been related to increased river inflow (Leroy, 2001; Mertens et al., 2009a). With regard to the rates of change, it should be noted that process length variation in the westernmost core MAR02-45P does not show a distinct lag behind the more eastern cores GeoB7625-2 and MAR05-13P (Fig. 4), as previously suggested by Verleye et al. (2009) and Mudie et al. (2009) based on differences in assemblage composition. The revised age model for MAR02-45P and GeoB7625-2 presented in this paper eliminates this previously suggested discrepancy.

5.3. Application of regional salinity reconstruction to cores in the Black Sea

The use of the equation in Fig. 6 allows reconstruction of the regional annual salinity record from the regional average process length for the time interval from 9.9 to 0.0 cal ka BP, with a time-step of 10 years (Fig. 7). This record shows a very gradual change from salinities of about 14 psu after the first reconnection at 9.14 cal ka BP, to minimum salinities of about 12.3 psu at 8.5 cal ka BP, reaching current conditions of about 17.1 psu at around 4.1 cal ka BP. The estimated maximum change in salinity during this period is thus $\sim 4.8 \pm 0.91$ psu.

Our salinity quantification for the lower (early Holocene) sedimentary unit (equivalent to Unit 2 of Wall and Dale, 1973) falls within the qualitative estimate of ~7–18 psu made by Wall and Dale (1973) and values of ~14–18 psu derived by Mudie et al. (2001) from correlation between relative abundances of cyst process types (normal or short form) and salinity estimates based on $\delta^{18}O$ values for the tests of planktonic foraminifera from the eastern Marmara Sea near the Strait of Bosphorus entrance to the Black Sea. Corresponding values previously estimated for late Holocene coccolith-rich sediments (equivalent to the Black Sea basin Unit 1) are ~18–22 psu (Wall and Dale, 1973) and ~18–20 psu (Mudie et al., 2001). Wall and Dale (1973) commented that vertical changes of cysts assemblages within sediments of Units 2 and 1 of deep Black Sea basin cores apparently reflect an increase in salinity from 7 to 18 psu, but the low resolution assemblage data do not indicate whether or not the salinity rose gradually and steadily during this time or increased through a series of pulsating increments as inferred from mollusk, ostracod and benthic foraminiferal data (e.g. Yanko-Hombach, 2007).

The salinity of the section below our studied interval was estimated as <7 psu by Wall and Dale (1973) and 4–12 psu by Mudie et al. (2004), based on cyst assemblage composition; Marret et al. (2009) suggested it was deposited in low salinities of ~7–12 psu, based on dinoflagellate cyst assemblages compared with modern Caspian Sea assemblages. Unfortunately, the sparsity or absence of *L. machaerophorum* in this section does not allow use of our process-length salinity proxy for environments where salinity is persistently <10 psu, probably because culture experiments (Hallett, 1999) show that *L. polyedrum* does not survive salinities below 10 psu. In the Black Sea cores studied here, *L. machaerophorum* is absent in

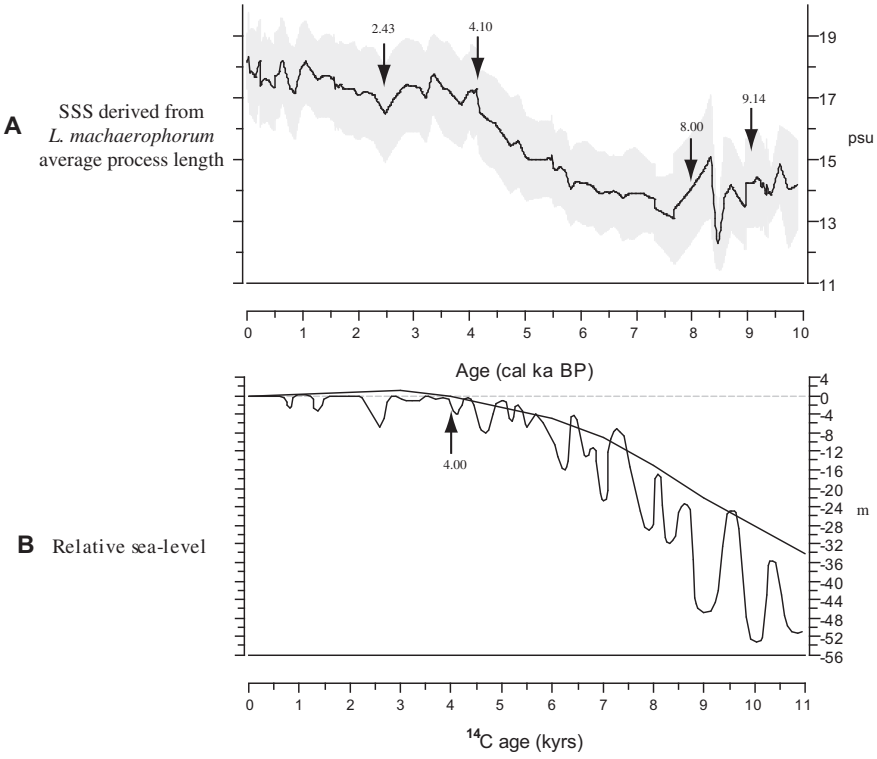

Fig. 7. A. Reconstruction of regional Black Sea annual salinity based on the average regional process length of *Lingulodinium machaerophorum* with a time-step of 10 years, using calibrated ages (cal ka BP). The sampling interval of the original cores is ~250 years, as illustrated in Fig. 4. The gray shading represents the calculated standard deviation. B. Relative sea-level variations after Balabanov (2007) and interpolated curve after Brückner et al. (2010), using ^{14}C ages (ka). Note that ages for this curve are uncalibrated. Arrows in A and B indicate the age of Ryan et al. (2003) flood at ~9.14 cal ka BP, the onset of two-way flow at ~8.0 cal ka BP, the moment when current salinities and current relative sea-level are reached (respectively 4.1 cal ka BP and 4.00 ^{14}C ka) and the first invasion of *Emiliania huxleyi* at 2.43 cal ka BP (Jones and Gagnon, 1994).

Pre-boreal – Holocene sediments, although rare short-process bearing cysts occur in samples with an age of about 19 ^{14}C ka in early MIS2 and 33.5 ^{14}C ka in MIS 3 (Mudie et al., 2004 and unpublished data from the Black Sea Atlantis II core 1479 previously studied by Wall and Dale (1973)). The dominant dinoflagellate cysts in this oldest section are *Spiniferites cruciformis* and *Pyxidinopsis psilata*, which occur in the recent Caspian Sea and in Lake Sapanca (Leroy et al., 2009) but little is known about their ecology (Marret et al., 2004) except for the correlation between *S. cruciformis* and salinity estimates of <14 psu derived from δ^{18}O values for the tests of co-occurring planktonic foraminifera (Mudie et al., 2001). Studies on the ecology and morphological variations of these now rare species are needed to refine our paleosalinity record and fully assess the amplitude and rate of surface salinity change before about 9.9 cal ka BP.

5.4. Paleoclimatological implications

Sea surface salinity changes in the Black Sea are currently regulated by the precipitation–evaporation budget (P–E), continental run-off, sea-level variations and changes in the two-way flow. All these factors are strongly intertwined: for example changes in the P–E budget strongly influence the two-way flow. During the early Holocene, high precipitation would have strengthened the outflow: an early to mid Holocene wet period (between 10.5 and 5.4 cal ka BP) is recorded in pollen records for MAR02-45P (Mudie et al., 2007) and, south of our core sites in the varved δ^{18}O speleothem record for Sofular Cave, that tracks the isotopic signature of Black Sea surface water (Badertscher et al., 2011; Göktürk et al., 2011). This enhanced rainfall was suggested to have caused a 3 psu drop in salinity in the northern Red Sea (Arz et al., 2003) and has probably kept the early Holocene salinity low despite the ongoing sea-level rise. After this initial period, our palaeosalinity reconstruction is similar to a the smoothed relative sea-level curve of Balabanov (2007) derived from paleogeographical data ground-truthed by micropaleontological methods and subsequently interpolated by Brückner et al. (2010. their Fig. 7, line B), reaching current sea-levels at about 4000 ^{14}C BP, (ca 4.1 cal ka BP; compare Fig. 7A and B). This coincident timing suggest that changes in global sea-level can be considered the dominant factor in causing salinity changes in the Black Sea after the humid early Holocene.

Following full reconnection and persistent two-way flow between the Marmara and Black seas, here dated at about 8.0 cal ka, the modern surface conditions of about 17.1 psu were reached at around 4.1 cal ka BP (Fig. 7A). The estimated gradual change in salinity during these ~3850 years is thus ~4.8 ± 0.91 psu. This surface water salinity change is much smaller and faster than the ~20 psu change in ca 7000 yr suggested by Soulet et al. (2010) for bottom water salinity using pore-water chloride profiles from sites ~50 km seaward of the lowstand Danube Delta and a diffusion–advection model. Soulet et al. (2010) suggested that the glacial Black Sea was a "freshwater" lake with bottom-water salinities of ~1 psu, only reaching modern bottom-water salinities of ~22 psu at 2 cal ka BP. They attribute this lengthy delay of 7000 yr in salinization to higher precipitation during the early Holocene. Caution is required in assessing the Soulet et al. (2010) interpretation that fresh pore-water being expelled upward from compacting muddy sediments reflects the composition of late Pleistocene and early Holocene Black Sea water. In an analogous setting off the US east coast, fresh pore-waters beneath the continental shelf are potentially relict freshwater lenses in aquifers that developed during Pleistocene lowstands (Kohout et al., 1977, their hypothesis 3); low sediment permeabilities have dramatically delayed the replacement of this freshwater by modern overlying saline water. The existence of such aquifers off the Danube Delta needs evaluation. In our study, the relatively small change in salinity values (~4.8 psu variation) suggests much less dramatic changes in ocean chemistry than proposed by Soulet et al. (2010). The 3850 years of salinity change in our study is in between the values of 3700 and 4800 years suggested by models using, respectively, the modern and double the modern freshwater input (10000 and 20000 m^3/s), with a sill depth of 40 m (Lane-Serff et al., 1997).

The similarity in timing of our Black Sea summer salinity record to average global sea-level (Fig. 7A and B) rise suggests that sea-level variation is the main driver in determining the end of the delay in surface salinization during the early-mid Holocene. Distinct lower frequency cycles cannot be observed in our salinity reconstruction, in contrast to the original sea-level curve of Balabanov (2007) and the benthic foraminiferal data of Martin and Yanko-Hombach (2011) (Fig. 7A and B). This lack of any distinct peaks or troughs (wiggles) of significant amplitude suggests that no catastrophic flood(s) occurred within the time-frame of our data. Catastrophic is defined here as 'very rapid (annual-decadal scale), irreversibly destructive events; any large and disastrous event of great significance; a disaster beyond expectations', following Yanko-Hombach et al. (2010) and Grishin (2001). In the original hypothesis of Ryan et al. (1997), the catastrophic flood would have occurred in less than 2 years. Modeling experiments by Myers et al. (2003) show that this short time would not have been possible and that at least one decade would be needed to realize the salinity change proposed by Ryan et al. (1997). Recent work also suggests that the Black Sea level at the time of the catastrophic flood could not have been more than 30 m below the present sea level, much less than the 50 m previously proposed (Giosan et al., 2011). Soulet et al. (2010, Table 1, p. 61) suggest that such a catastrophic event would result in a sudden salinity increase of ~2 psu. There is no evidence for such catastrophic, abrupt and consistent increase in salinity at the "Flood age" around ~9.14 cal ka BP (using our calibration procedures) within the ~250 year resolution of our samples (Figs. 4 and 7). The reconstruction based on the process lengths of *L. machaerophorum* thus contradicts the catastrophic Noah's flood hypothesis of Ryan et al. (2003) and supports a gradual Holocene incursion of saline Mediterranean water into the Black Sea.

The paleosalinity record also reveals that there is no simple relation between salinity and the occurrence of the coccolith *E. huxleyi* in the Black Sea. Current conditions of about 17.1 psu at around 4.1 cal ka BP were reached ~1700 years before the start of the first large invasion of *E. huxleyi*, dated at approximately 2.43 ± 0.20 cal ka BP (Table 1; after Jones and Gagnon, 1994), although *E. huxleyi* was present in trace amounts during the early Holocene (Giunta et al., 2007). The discovery of mid-early Holocene occurrences of *E. huxleyi* fossil DNA in the Black Sea (Coolen et al., 2009) reinforces the interpretation that the coccolith blooms resulted from increased shipping trade between the Mediterranean Sea and Black Sea (Jones and Gagnon, 1994). We did not observe any coincident freshening of surface water during the late Holocene interval of coccolith deposition, contrary to the observation of van der Meer et al. (2008) using δD in alkenones. This discrepancy may be related to either local effects or issues with the δD alkenone technique (e.g. Schwab and Sachs, 2011).

It should also be noted that in the Marmara Sea, although dinoflagellate cyst records (Mudie et al., 2002, 2004; Londeix et al., 2009) and benthic foraminifera (Kaminski et al., 2002; McHugh et al., 2008) show relatively low salinity during the early-mid Holocene interval of sapropelic mud deposition, some Holocene salinity reconstructions show an opposite trend to our Black Sea reconstruction: high salinities during the early Holocene and low salinities during the mid Holocene were reported by Sperling et al. (2003) and by Vidal et al. (2010), based on planktonic foraminifera and ostracod geochemistry, respectively. This pattern was explained

as accumulation of relatively warm saline Mediterranean waters during the early Holocene in the Marmara Sea before overflow of low salinity water from the Black Sea after 9.14 cal ka and subsequent increased outflow from the Black Sea (Sperling et al., 2003). However, the geochemistry of the early-mid Holocene sapropel in the Marmara Sea has a primary marine signal while the early Holocene interval shows a strong terrigenous geochemical signal, implying some outflow of Black Sea water (Vidal et al., 2010).

6. Conclusions

This study documents the morphological variation of *L. machaerophorum* extracted from surface sediments from the Black Sea, the Kerch Strait at the exit of the Sea of Azov, the Caspian Sea and Marmara Sea, and from 6 Holocene sediment cores in the Black Sea. A molecular investigation of SSU, LSU and ITS sequences from cysts from the Caspian and Black seas shows that despite morphological differences, the cysts correspond to the same species and are also the same as cultures established from cysts from California. Furthermore, this suggests that strain-specific responses are not a plausible factor in process length. Average process length (PL) of *L. machaerophorum* in 60 surface samples is correlated to annual surface water salinity through the equation: $SSS_{summer} = 0.026^{*}PL^{2} - 0.0145PL + 12.136$ ($R^2 = 0.91$). This equation can be applied to reconstruct surface salinity quantitatively with a precision of $\pm$0.91 psu in the Black Sea, at least in the range between 11.9 and 22.2 psu. A regional quantitative salinity reconstruction is shown for a ca 9.9 cal ka record obtained by interpolating sediment ages and averaging measured process lengths from the 6 late Quaternary cores taken from 4 different cores sites in the Black Sea. We show that the salinity increase after the earliest Holocene was gradual, and ranged from 12.3 to 17.1 psu ($\sim 4.8 \pm 0.91$ psu). This is the first quantitative high-resolution regional paleosalinity record using the process length of the dinoflagellate cyst *L. machaerophorum*. After an early period of low salinities related to enhanced precipitation, the salinity-proxy does not record large Holocene salinity fluctuations and shows correspondence to the regional sea-level curve of Balabanov (2007), as interpolated by Brückner et al. (2010), and suggests a dominant influence of sea-level variations on salinity change in the Black Sea during the late Holocene.

Acknowledgments

Kenneth N. Mertens is a Postdoctoral scholar of FWO Belgium. This research was conducted by the lead author at Nagasaki University, Japan thanks to a JSPS fellowship. Financial support to Thomas J. Verleye was provided by the Institute for the Encouragement of Innovation through Science and Technology in Flanders (IWT). Petra Mudie, Ali Aksu, Richard Hiscott and Vera Pospelova are grateful for financial support from the Natural Sciences and Engineering Research Council of Canada (NSERC). Lee Bradley and Fabienne Marret thank the Leverhulme Trust for financial support. The officers and crew of RV *Koca Piri Reis* are thanked for facilitating the collection of the MAR cores in 2002 and 2005. Petra Mudie, Lee Bradley and Fabienne Marret acknowledge the help of Helen Gillespie, Memorial University of Newfoundland, in processing of samples from the MAR cores. Anna Linegar helped calibrate raw ^{14}C dates. Dr. Marcel van der Meer (NIOZ) is thanked for providing samples of boxcore BC53. Jennifer Cranshaw is acknowledged for clarifying the amount of core-top loss for MAR05-13P, and its correlation with MAR05-4G. We are grateful to Dr Igor Bondarev, National Academy of Science of Ukraine, Sevastopol, for diving to sample for living dinoflagellate cysts on the NW Black Sea shelf during INQUA 501 field trip 2. We thank Dennis Dunn, Adam Willingham, and Carrie Wolfe (the Southern California Marine Institute) for their assistance in sediment sampling in San Pedro Harbor, California. Neslihan Balkis is thanked for help with obtaining salinity data and Helmut Brückner for communications on sea-level variations in the Black Sea. The comments of wo anonymous reviewers were appreciated.

Appendix. Supplementary material

Supplementary material associated with this article can be found, in the online version, at doi:10.1016/j.quascirev.2012.01.026.

References

Aksu, A.E., Hiscott, R.N., Mudie, P.J., Rochon, A., Kaminski, M.A., Abrajano, T., Yaşar, D., 2002a. Persistent Holocene outflow from the Black Sea to the Eastern Mediterranean contradicts Noah's Flood hypothesis. GSA Today 12, 4–9.

Aksu, A.E., Hiscott, R.N., Yaşar, D., Işler, F.I., Marsh, S., 2002b. Seismic stratigraphy of Late Quaternary deposits from the southwestern Black Sea shelf: evidence for non-catastrophic variations in sea-level during the last ~10000 yr. Marine Geology 190, 61–94.

Arz, H.W., Lamy, F., Pätzold, J., Müller, P.J., Prins, M., 2003. Mediterranean moisture source for an early-Holocene humid period in the northern Red Sea. Science 300, 118–121.

Badertscher, S., Fleitmann, D., Cheng, H., Edwards, R.L., Göktürk, O.M., Zumbühl, A., Leuenberger, M., Tüysüz, O., 2011. Pleistocene water intrusions from the Mediterranean and Caspian seas into the Black Sea. Nature Geoscience 4, 236–239.

Bagheri, S., Mansor, M., Makaremi, M., Mirzajani, A., Babaei, H., Negarestan, H., Maznah, W., 2010. Distribution and composition of phytoplankton in the Southwestern Caspian Sea during 2001-2002, a comparison with previous surveys. World Journal of Fish and Marine Sciences 2 (5), 416–426.

Bahr, A., Arz, H.W., Lamy, F., Wefer, G., 2006. Late glacial to Holocene paleoenvironmental evolution of the Black Sea, reconstructed with stable oxygen isotope records obtained on ostracod shells. Earth and Planetary Science Letters 241, 863–875.

Balabanov, I.P., 2007. Holocene sea-level changes of the Black Sea. In: Yanko-Hombach, V., Gilbert, A.S., Panin, N., Dolukhanov, P.M. (Eds.), The Black Sea Flood Question. Springer, Dordrecht, pp. 711–730.

Balkis, N., 2003. Seasonal variations in the phytoplankton and nutrients dynamics in the neritic water of Büyükçekmece Bay, Sea of Marmara. Journal of Plankton Research 25 (7), 703–717.

Beşiktepe, S., Sur, H.I., Özsoy, E., Latif, M.A., Oğuz, T., Ünlüata, Ü., 1994. The circulation and hydrography of the Marmara Sea. Progress in Oceanography 34, 285–334.

Bolch, C.J.S., 1997. The use of polytungstate for the separation and concentration of living dinoflagellate cysts from marine sediments. Phycologia 37, 472–478.

Brenner, W., 2005. Holocene environmental history of the Gotland Basin (Baltic Sea) – a micropalaeontological model. Palaeogeography, Palaeoclimatology, Palaeoecology 220, 227–241.

Brückner, H., Kelterbaum, D., Marunchak, O., Porotov, A., Vött, A., 2010. The Holocene sea level story since 7500 BP – lessons from the Eastern Mediterranean, the Black and the Azov Seas. Quaternary International 225, 160–179.

Cagatay, M.N., Görür, N., Algan, O., Eastoe, C., Tchapalyga, A., Ongan, D., Kuhn, T., Kuscu, I., 2000. Late Glacial-Holocene palaeoceanography of the Sea of Marmara: timing of connections with the Mediterranean and the Black Seas. Marine Geology 167, 191–206.

Caner, H., Algan, O., 2002. Palynology of sapropelic layers from the Marmara Sea. Marine Geology 190, 35–46.

Coolen, M.J.L., Saenz, J.P., Giosan, L., Trowbridge, N.Y., Dimitrov, P., Dimitrov, D., Eglinton, T.I., 2009. DNA and lipid molecular stratigraphic records of haptophyte succession in the Black Sea during the Holocene. Earth and Planetary Science Letters 284, 610–621.

Cranshaw, J., 2007. Carbon and sulphur elemental and isotopic results from coring of a long piston core on the southwestern Black Sea shelf, Sakarya region: implications for communication between the Black Sea and eastern, Mediterranean Sea during the last 10,000 years. Honours B.Sc. Thesis, Memorial University of Newfoundland, St. John's, Canada, 59 pp.

Dale, B., 1996. Dinoflagellate cyst ecology: modelling and geological applications. In: Jansonius, J., McGregor, D.C. (Eds.), 1996. Palynology: Principles and Applications, vol. 3. AASP Foundation, Dallas, pp. 1249–1275.

Ellegaard, M., 2000. Variations in dinoflagellate cyst morphology under conditions of changing salinity during the last 2000 years in the Limfjord, Denmark. Review of Palaeobotany and Palynology 109, 65–81.

Eremeev, V.P., Ivanov, V.A., Ilin Ju, P., 2003. Oceanographic conditions and environmental challenges of the Kerch Strait. Marine Ecological Journal 3 (2), 27–39 (in Russian).

Friedrich, W.L., Kromer, B., Friedrich, M., Heinemeier, J., Pfeiffer, T., Talamo, S., 2006. Science 312 (5773), 548.

Frommlet, J.C., Eglesias-Rodriguez, M.D., 2008. Microsatellite genotyping of single cells of the dinoflagellate species *Lingulodinium polyedrum* (Dinophyceae): a novel approach for marine microbial population genetic studies. Journal of Phycology 44, 1116–1125.

Giosan, L., Filip, F., Constatinescu, S., 2011. Was the Black Sea catastrophically flooded in the early Holocene? Quaternary Science Reviews 28 (2009), 1–6.
Giunta, S., Morigi, C., Negri, A., Guichard, F., Lericolais, G., 2007. Holocene biostratigraphy and paleoenvironmental changes in the Black Sea based on calcareous nannoplankton. Marine Micropaleontology 63, 91–110.
Göktürk, O.M., Fleitmann, D., Badertscher, S., Cheng, H., Edwards, R.L., Leuenberger, M., Fankhauser, A., Tüysüz, O., Kramer, J., 2011. Climate on the southern Black Sea coast during the Holocene: implications from the Sofular Cave record. Quaternary Science Reviews 30, 2433–2445.
Grishin, A.M., 2001. Heat and mass transfer and modeling and prediction of environmental catastrophes. Journal of Engineering Physics and Thermophysics 74, 895–902.
Hallett, R.I., 1999. Consequences of Environmental Change on the Growth and Morphology of *Lingulodinium polyedrum* (Dinophyceae) in Culture. Ph.D. Thesis. University of Westminster, 109 pp.
Head, M.J., 2007. Last Interglacial (Eemian) hydrographic conditions in the southwestern Baltic Sea based on dinoflagellate cysts from Ristinge Klint, Denmark. Geological Magazine 144, 987–1013.
Hiscott, R.N., Aksu, A.E., Yaşar, D., Kaminski, M.A., Mudie, P.J., Kostylev, V.E., MacDonald, J.C., Işler, F.I., Lord, A.R., 2002. Deltas south of the Bosphorus Strait record persistent Black Sea outflow to the Marmara Sea since ~10 ka. Marine Geology 190 (1–2), 261–282.
Hiscott, R.N., Aksu, A.E., Mudie, P.J., Kaminski, M.A., Abrajano, T., Yaşar, D., Rochon, A., 2007a. The Marmara Sea Gateway since ~16 ka: non-catastrophic causes of paleoceanographic events in the Black Sea at 8.4 and 7.15 ka. In: Yanko-Hombach, V., Gilbert, A.S., Panin, N., Dolukhanov, P.M. (Eds.), The Black Sea Flood Question: Changes in Coastlines, Climate and Human Settlement. Springer, Dordrecht, pp. 89–117.
Hiscott, R.N., Aksu, A.E., Mudie, P.J., Marret, F., Abrajano, T., Kaminski, M.A., Evans, J., Çakiroğlu, A.I., Yaşar, D., 2007b. A gradual drowning of the southwestern Black Sea shelf: evidence for a progressive rather than abrupt Holocene reconnection with the eastern Mediterranean Sea through the Marmara Sea Gateway. Quaternary International 167, 19–34.
Hiscott, R.N., Aksu, A.E., Mudie, P.J., Marret, F., Abrajano, T., Kaminski, M.A., Evans, J., Çakiroğlu, A.I., Yaşar, D., 2010. Corrigendum to "A gradual drowning of the southwestern Black Sea shelf: evidence for a progressive rather than abrupt Holocene reconnection with the eastern Mediterranean Sea through the Marmara Sea Gateway" [Quaternary International, 167–168 (2007) 19–34]. Quaternary International 226 (1–2), 160.
Il'in, G.V., Moiseev, D.V., Belyaev, A.G., 2001. Modern Features and Characteristic Peculiarities of Hydrological – Hydrochemical Regime of the Azov Sea Coastal Waters" in Environment, Biota and Modelling of Ecological Processes in the Azov Sea (KNTs RAN, Apatity, 2001), pp. 17–33 (in Russian).
Jones, G.A., Gagnon, A.R., 1994. Radiocarbon chronology of Black Sea sediments. Deep-sea Research I 41 (3), 531–557.
Kaminski, M.A., Aksu, A., Box, M., Hiscott, R.N., Filipescu, S., Al-Salameen, M., 2002. Late Glacial to Holocene benthic foraminifera in the Marmara Sea: implications for Black Sea–Mediterranean Sea connections following the last deglaciation. Marine Geology 190 (1–2), 165–202.
Kara, A.B., Wallcraft, A.J., Hurlburt, H.E., Stanev, E.V., 2008. Air – sea fluxes and river discharges in the Black Sea with a focus on the Danube and Bosphorus. Journal of Marine Systems 74, 74–95.
Kohout, F.A., Hathaway, J.C., Folger, D.W., Bothner, M.H., Walker, E.H., Delaney, D.F., Frimpter, M.H., Weed, E.G.A., Rhodehamel, E.C., 1977. Fresh ground water stored in aquifers under the continental shelf: implications from a deep test, Nantucket Island, Massachusetts. Water Resources Bulletin 13, 373–386.
Kokinos, J.P., Anderson, D.M., 1995. Morphological development of resting cysts in cultures of the marine dinoflagellate *Lingulodinium polyedrum* (=*L. machaerophorum*). Palynology 19, 143–166.
Kosarev, A.N., Yablonskaya, E.A., 1994. The Caspian Sea. SPB Academic Publishing, The Hague.
Kwiecien, O., Arz, H.W., Lamy, F., Wulf, S., Bahr, A., Röhl, U., Haug, G.H., 2008. Estimated reservoir ages of the Black Sea since the Last Glacial. Radiocarbon 50 (1), 99–118.
Lamy, F., Arz, H.W., Bond, G.C., Bahr, A., Pätzold, J., 2006. Multicentennial-scale hydrological changes in the Black Sea and northern Red Sea during the Holocene and the Arctic/North Atlantic Oscillation. Paleoceanography 21, PA1008. doi:10.1029/2005PA001184.
Lane-Serff, G.F., Rohling, E.J., Bryden, H.L., Charnock, H., 1997. Postglacial connection of the Black Sea to the Mediterranean and its relation to the timing of sapropel formation. Paleoceanography 12 (2), 169–174.
Latif, M.L., Özsoy, E., Salihoğlu, I., Gaines, A.F., Baştürk, Ö., Yılmaz, A., Tuğrul, S., 1992. Monitoring via Direct Measurements of the Modes of Mixing and Transport of Wastewater Discharges into the Bosphorus Underflow. Middle East Technical University, Institute of Marine Sciences, Technical Report, No 92-2, 98 p.
Leroy, S.A.G., Marret, F., Giralt, S., Bulatov, S.A., 2006. Natural and anthropogenic rapid changes in the Kara-Bogaz Gol over the last two centuries reconstructed from palynological analyses and a comparison to instrumental records. Quaternary International 150, 52–70.
Leroy, S.A.G., Boyraz, S., Gürbüz, A., 2009. High-resolution palynological analysis in Lake Sapanca as a tool to detect recent earthquakes on the North Anatolian Fault. Quaternary Science Reviews 28, 2616–2632.
Leroy, V., 2001. Traceurs palynologiques des flux biogéniques et des conditions hydrographiques en milieu marin cotier: exemple de l'étang de Berre. DEA, Ecole doctorale Sciences de l'environment d'Aix-Marseille, 30 pp.
Lewis, J., Hallett, R., 1997. Lingulodinium polyedrum (Gonyaulax polyedra) a blooming dinoflagellate. In: Ansell, A.D., Gibson, R.N., Barnes, M. (Eds.), 1997. Oceanography and Marine Biology: an Annual Review, vol. 35. UCL Press, London, pp. 97–161.
Locarnini, R.A., Conkright, M.E., Boyer, T.P., Antonov, J.I., Baranova, O.K., Garcia, H.E., Gelfeld, R., Johnson, D., Murphy, P.P., O'Brien, T.D., Smolyar, I., 2002. World Ocean Database 2001, volume 4: Temporal distribution of temperature, salinity, and oxygen profiles. In: Levitus, S. (Ed.), 2002. NOAA Atlas NESDIS, vol. 45. U.S. Government Printing Office, Wash., D.C, p. 332. CD-ROM.
Londeix, L., Herreyre, Y., Turon, J.L., Fletcher, W., 2009. Last Glacial to Holocene hydrology of the Marmara Sea inferred from a dinoflagellate cyst record. Review of Palaeobotany and Palynology 158, 52–71.
Marret, F., Leroy, S.A.G., Chalié, F., Gasse, F., 2004. New organic-walled dinoflagellate cysts from recent sediments of Central Asian seas. Review of Palaeobotany and Palynology 129, 1–20.
Marret, F., Mudie, P., Aksu, A., Hiscott, R.N., 2009. A Holocene dinocyst record of a two-step transformation of the Neoeuxinian brackish water lake into the Black Sea. Quaternary International 193, 72–86.
Martin, R.E., Yanko-Hombach, V., 2011. Rapid Holocene sea-level and climate change in the Black Sea: and evaluation of the Balabonov sea-level curve. In: Buyenevich, I.V., Yanko-Hombacg, V., Gilbert, A.S., Martin, R.E. (Eds.), 2011. Geology and Geoarchaeology of the Black Sea Region: Beyond the Flood Hypothesis. Geological Society of America Special Paper, vol. 473, pp. 51–58.
Matishov, G.G., Abramenko, M.M., Gargopa, Y.M., Bufetova, M.V., 2003. The Newest Ecological Phenomena in the Azov Sea (Second Half of the XX Century) (KNTs RAN, Apatity) (in Russian).
Matthiessen, J., Brenner, W., 1996. Chlorococcalalgen und Dinoflagellaten-Zysten in rezenten Sedimenten des Greifswalder Boddens (südliche Ostsee). Senckenbergiana Maritima 27, 33–48.
McHugh, C.M., Gurung, D., Giosan, L., Ryan, W.B.F., Mart, Y., Sancar, U., Burckle, L., Cağatay, M.N., 2008. The last reconnection of the Marmara Sea, Turkey to the World Ocean: a paleoceanographic and paleoclimatic perspective. Marine Geology 255, 64–82.
MEDAR Group, 2002. MEDATLAS/2002 Database. Mediterranean and Black Sea Database of Temperature Salinity and Bio-chemical Parameters. Climatological Atlas. IFREMER Edition (4 Cdroms).
Mertens, K.N., Ribeiro, S., Bouimetarhan, I., Caner, H., Combourieu-Nebout, N., Dale, B., de Vernal, A., Ellegaard, M., Filipova, M., Godhe, A., Grøsfjeld, K., Holzwarth, U., Kotthoff, U., Leroy, S., Londeix, L., Marret, F., Matsuoka, K., Mudie, P., Naudts, L., Peña-manjarrez, J., Persson, A., Popescu, S., Sangiorgi, F., van der Meer, M., Vink, A., Zonneveld, K., Vercauteren, D., Vlassenbroeck, J., Louwye, S., 2009a. Process length variation in cysts of a dinoflagellate, Lingulodinium machaerophorum, in surface sediments investigating its potential as salinity proxy. Marine Micropaleontology 70, 54–69.
Mertens, K.N., González, C., Delusina, I., Louwye, S., 2009b. 30 000 years of productivity and salinity variations in the late Quaternary Cariaco Basin revealed by dinoflagellate cysts. Boreas 38, 647–662.
Mertens, K.N., Dale, B., Ellegaard, M., Jansson, I.-M., Godhe, A., Kremp, A., Louwye, S., 2010. Process length variation in cysts of the dinoflagellate Protoceratium reticulatum, from surface sediments of the Baltic–Kattegat–Skagerrak estuarine system: a regional salinity proxy. Boreas. doi:10.1111/j.1502–3885.2010.00193.x.
Mudie, P.J., Aksu, A.E., Yaşar, D., 2001. Late Quaternary dinoflagellate cysts from the Black, Marmara and Aegean seas: variations in assemblages, morphology and paleosalinity. Marine Micropaleontology 43, 155–178.
Mudie, P.J., Rochon, A., Aksu, A.E., Gillespie, H., 2002. Dinocysts, freshwater algae and fungal spores as salinity indicators in Late Quaternary cores from Marmara and Black seas. Marine Geology 190, 203–231.
Mudie, P.J., Rochon, A., Aksu, A.E., Gillespie, H., 2004. Late glacial, Holocene and modern dinoflagellate cyst assemblages in the Aegean–Marmara–Black Sea corridor: statistical analysis and re-interpretation of the early Holocene Noah's Flood hypothesis. Review of Palaeobotany and Palynology 128 (1–2), 143.
Mudie, P.J., Marret, F., Aksu, A.E., Hiscott, R.N., Gillespie, H., 2007. Palynological evidence for climatic change, anthropogenic activity and outflow of Black Sea water during the Late Pleistocene and Holocene: centennial- to decadal-scale records from the Black and Marmara Seas. Quaternary International 167–168, 73–90.
Mudie, P.J., Mertens, K., Marret F., Verleye T., Aksu A.E., Hiscott R.N., 2009. Palynological signals of recent anthropogenic impacts on the Black Sea and the implications for early Holocene salinity changes. IGCP 521 – INQUA 0501 Fifth Plenary Meeting İzmir-Çanakkale, Turkey, 22–31 August 2009, Extended Abstracts, 123–125 pp.
Murray, W., Jannasch, H.W., Honjo, S., Anderson, F., Reeburgh, W.S., Top, Z., Friederich, E., Codispoti, L.A., Izdar, E., 1989. Unexpected changes in the oxic/anoxic interface in the Black Sea. Nature 338, 411–413.
Murray, J.W, 1991. Hydrographic variability in the Black Sea. In: Izdar, E., Murray, J.W. (Eds.), 1991. Black Sea Oceanography. NATO ASI Series, Series C: Mathematical and Physical Sciences, vol. 351. Kluwer Academic Publishers, London, pp. 1–15.
Myers, P.G., Wielki, C., Goldstein, S.B., Rohling, E.J., 2003. Hydraulic calculations of postglacial connections between the Mediterranean and the Black Sea. Marine Geology 201 (2003), 253–267.
Nehring, S., 1997. Dinoflagellate resting cysts from recent German coastal sediments. Botanica Marina 40, 307–324.
Oğuz, T., Latun, V.S., Latif, M.A., Vladimirov, V.V., Sur, H.I., Markov, A.A., Özsoy, E., Kotovshchikov, B.B., Eremeev, V.V., Ünlüata, Ü., 1993. Circulation in the surface and intermediate layers in the Black Sea. Deep-Sea Research 40, 1597–1612.

Özsoy, E., Latif, M.A., Tuğrul, S., Ünlüata, Ü., 1995. Exchanges with the Mediterranean, fluxes and boundary mixing processes in the Black Sea. In: Briand, F. (Ed.), Mediterranean Tributary Seas. Bulletin de l'Institut Océanographique, Monaco. Special No 15, CIESME Science Series 1, Monaco, pp. 1–25.

Polat, Ç., Tuğrul, S., 1996. Chemical exchange between the Mediterranean and Black Sea via the Turkish Straits. In: Briand, F. (Ed.), Dynamics of Mediterranean Straits and Channels. Bulletin de l'Institue Océanographique, Monaco, Special No. 17, CIESME Science Series 2, Monaco, pp. 167–186.

Rodionov, S.N., 1994. Global and Regional Climatic Interaction: the Caspian Sea Experience. Kluwer Academic Publishing, Dordrecht.

Ross, D.A., Degens, E.T., 1974. Recent sediments of Black Sea. In: Degens, E.T., Ross, D.A. (Eds.), The Black Sea – Geology, Chemistry and Biology. American Association of Petroleum Geologists, Tulsa, Oklahoma, pp. 183–199.

Ryan, W.B.F., Pitman III, W.C., 1998. Noah's Flood: the New Scientific Discoveries about the Event that Changes History. Simon and Schuster, New York, 319 p.

Ryan, W.B.F., Pitman III, W.C., Major, C.O., Shimkus, K., Moskalenko, V., Jones, J.A., Dimitrov, P., Görür, N., Sakinç, M., Yüce, H., 1997. An abrupt drowning of Black Sea shelf. Marine Geology 138, 119–126.

Ryan, W.B.F., Major, C.O., Lericolais, G., Goldstein, S., 2003. Catastrophic flooding of the Black Sea. Annual Review of Earth and Planetary Sciences 31, 525–554.

Schlitzer, R., 2010. Ocean Data View. http://odv.awi.de (accessed 01.03.10.).

Schwab, V.F., Sachs, J.P., 2011. Hydrogen isotopes in individual alkenones from the Chesapeake Bay estuary. Geochimica et Cosmochimica Acta. doi:10.1016/j.gca.2011.09.031.

Siani, G., Paterne, M., Arnold, M., Bard, E., Métivier, B., Tisnerat, N., Bassinot, F., 2000. Radiocarbon reservoir ages in the Mediterranean Sea and Black Sea. Radiocarbon 42 (2), 271–280.

Sorokin, Y.I., 2002. The Black Sea – Ecology and Oceanography. Backhuys Publishers, Leiden, 875 pp.

Sorrell, P., Popescu, S.M., Head, M.J., Suc, J.P., Klotz, S., Oberhänsli, H., 2006. Hydrographic development of the Aral Sea during the last 2000 years based on a quantitative analysis of dinoflagellate cysts. Palaeography, Palaeoclimatology, Palaeoecology 234, 304–327.

Soulet, G., Delaygue, G., Vallet-Coulomb, C., Böttcher, M.E., Sonzogni, C., Lericolais, G., Bard, E., 2010. Glacial hydrologic conditions in the Black Sea reconstructed using geochemical pore water profiles. Earth and Planetary Science Letters 296, 57–66.

Soulet, G., Ménot, G., Garreta, V., Rostek, F., Zaragosi, S., Lericolais, G., Bard, E., 2011. Black Sea "Lake" reservoir age evolution since the Last Glacial – Hydrologic and climatic implications. Earth and Planetary Science Letters 308, 245–258.

Sperling, M., Schmiedl, G., Hemleben, C., Emeis, K.C., Erlenkeuser, H., Grootes, P.M., 2003. Black Sea impact on the formation of eastern Mediterranean sapropel S1? Evidence from the Marmara Sea. Palaeography, Palaeoclimatology, Palaeoecology 190, 9–21.

Stanev, E.V., 2005. Understanding Black Sea dynamics, an overview of recent numerical modelling. Oceanography 18, 56–75.

Takano, Y., Horiguchi, T., 2005. Acquiring scanning electron microscopical, light microscopical and multiple gene sequence data from a single dinoflagellate cell. Journal of Phycology 42 (1), 251–256.

Türkoğlu, M., Koray, T., 2002. Phytoplankton species succession and nutrients in the Southern Black Sea (Bay of Sinop). Turkish Journal of Botany 26, 235–252.

UNEP, 2006. Stolberg, F., Borysova, O., Mitrofanov, I., Barannik, V. and Eghtesadi, P., Caspian Sea, GIWA Regional Assessment 23. University of Kalmar, Kalmar, Sweden.

van der Meer, M.T.J., Sangiorgi, F., Baas, M., Brinkhuis, H., Sinninghe-Damsté, J.S., Schouten, S., 2008. Molecular isotopic and dinoflagellate evidence for Late Holocene freshening of the Black Sea. Earth and Planetary Science Letters 267, 426–434.

Verleye, T.J., Mertens, K.N., Louwye, S., Arz, H.W., 2009. Holocene salinity changes in the southwestern black sea: a reconstruction based on dinoflagellate cysts. Palynology 33, 77–100.

Vidal, L., Ménot, G., Joly, C., Bruneton, H., Rostek, F., Cağatay, M.N., Major, C., Bard, E., 2010. Hydrology in the Sea of Marmara during the last 23 ka: implications for timing of Black Sea connections and sapropel deposition. Paleoceanography 25, PA1205,. doi:10.1029/2009PA001735.

Wall, D., Dale, B., 1973. Palaeosalinity relationships of dinoflagellates in the Late Quaternary of the Black Sea – a summary. Geosciences and Man VII, 95–102.

Wall, D., Dale B., 1974. Dinoflagellates in Late Quaternary deep-water sediments of Black Sea: biology. AAPG Special Volumes Volume 20: The Black Sea – Geology, Chemistry, and Biology, 364–380 pp.

Wall, D., Dale, B., Harada, K., 1973. Description of new fossil dinoflagellates from the Late Quaternary of the Black Sea. Micropaleontology 19, 18–31.

Yanko-Hombach, V., Mudie, P., Gilbert, A.S., 2010. Was the Black Sea catastrophically flooded during the Holocene? – geological evidence and archaeological impacts. In: Benjamin, J., Bonsall, C., Pickard, C., Fischer, A. (Eds.), Submerged Prehistory. Oxbow books, pp. 245–262.

Yanko-Hombach, V., 2007. Controversy over Noah's Flood in the Black Sea: geological and foraminiferal evidence from the shelf. In: Yanko-Hombach, V., Gilbert, A.S., Panin, N., Dolukhanov, P.M. (Eds.), The Black Sea Flood Question. Springer, Dordrecht, pp. 149–204.

Zenkevitch, L.A., 1963. Biology of the Seas of the USSR. Moscow. (in Russian).